USE OF A THERMODYNAMIC CYCLE SIMULATION TO DETERMINE THE DIFFERENCE BETWEEN A PROPANE-FUELLED ENGINE AND AN ISO-OCTANE-FUELLED ENGINE

A Thesis

by

DUSHYANT PATHAK

Submitted to the Office of Graduate Studies of
Texas A&M University
in partial fulfillment of the requirements for the degree of

MASTER OF SCIENCE

December 2005

Major Subject: Mechanical Engineering

USE OF A THERMODYNAMIC CYCLE SIMULATION TO DETERMINE THE DIFFERENCE BETWEEN A PROPANE-FUELLED ENGINE AND AN ISO-OCTANE-FUELLED ENGINE

A Thesis

by

DUSHYANT PATHAK

Submitted to the Office of Graduate Studies of
Texas A&M University
in partial fulfillment of the requirements for the degree of

MASTER OF SCIENCE

Approved by:

Chair of Committee,	Jerald A. Caton
Committee Members,	Thomas R. Lalk
	Angie H. Price
Head of Department,	Dennis O' Neal

December 2005

Major Subject: Mechanical Engineering

ABSTRACT

Use of a Thermodynamic Cycle Simulation to Determine the Difference Between a Propane-fuelled Engine and an Iso-octane-fuelled Engine. (December 2005)

Dushyant Pathak, B.Tech., Kurukshetra University

Chair of Advisory Committee: Dr. Jerald A. Caton

A thermodynamic cycle simulation of the four-stroke spark-ignition engine was used to determine the effects of variations in engine design and operating parameters on engine performance and emission characteristics. The overall objective was to use the engine cycle simulation to determine the difference between a propane-fuelled and an iso-octane-fuelled engine for the same operating conditions and engine specifications.

A comprehensive parametric investigation was conducted to examine the effects of variations in load, speed, combustion duration, spark timing, equivalence ratio, exhaust gas recycle, and compression ratio for a 3.3 liter, Chrysler Minivan, V 6 engine operating on propane. Parameters were selected for the analysis. Variations in the brake specific fuel consumption, brake specific NO_x emissions, and mean exhaust temperature were determined for both the propane-fuelled and the iso-octane-fuelled engines.

Brake specific fuel consumption and mean exhaust temperature values for the propane-fuelled engine were consistently lower (3 to 5 %) than the corresponding values for the iso-octane-fuelled engine. Fuel structure did not have a significant effect on brake specific nitric oxide emissions.

Predictions made from the simulation were compared with some of the available experimental results. Predicted brake torque and brake power showed acceptable quantitative agreement (less than 10 % variation) in the low engine speed range (1,000 to 3,000 rpm) and similar trends with the available experimental data.

DEDICATION

I would like to dedicate this thesis to my parents who have been a major influence in my life. They have supported me wholeheartedly in all my endeavors. I would also like to dedicate the thesis to my elder brother, who has been among my best friends and whose encouragement has kept me going throughout my academic life.

ACKNOWLEDGMENTS

I would like to thank my committee chair, Dr. Jerald A. Caton for his constant support and encouragement throughout the course of this work. He was instrumental in my finishing this work. I would also like to thank my committee members, Dr. Thomas R. Lalk and Dr. Angie H. Price, whose cooperation and support allowed me to finish this work within the various constraints of time and resources.

Finally, I would like to express my gratitude to everyone who helped and supported me in my current endeavor.

TABLE OF CONTENTS

Page

LIST OF FIGURES

FIGURE Page

FIGURE Page

FIGURE Page

LIST OF TABLES

1. INTRODUCTION

Development of vehicles to operate on non-petroleum fuels gained substantial momentum in response to the energy crisis of the 1970's. While petroleum will still remain the predominant transportation fuel for the foreseeable future, petroleum supplies are finite and are depleting at a fiercely rapid rate. Therefore, it is becoming increasingly important to contemplate the difficult transition to the new sources of energy.

During the last couple of decades of research, the chemical composition of the fuel utilized in the internal combustion engines has gained wide recognition as a significant factor in controlling emissions. It has been widely argued that improvements in the air quality can be realized by using vehicles that operate on natural gas, propane, methanol, ethanol or electricity, but introduction of these alternative-fuel vehicles presents enormous technical and economic challenges to the automobile industry. Indicators [**1**] point to the fact that there will be a shortfall of approximately 25% in the crude oil supplies relative to the demand in approximately a decade's time from now. There will, therefore, be a need for alternative fuels to fuel spark-ignition engines.

1.1 Alternative Fuels: Guiding Factors

The market penetration of a particular alternative fuel will be dictated by its ability to meet certain established end-user requirements. These requirements have become critical as a consequence of the decades of widespread availability and high performance provided by gasoline and diesel. The essential requirements are:

a) The availability and supply in required volumes and at convenient locations and all times.
b) No impairment of vehicle performance over the entire range of operating conditions.

This thesis follows the format and style of *Journal of Automobile Engineering*.

c) A level of safety similar or superior to the current levels of safety in refueling and general use of the fuel.
d) A vehicle range comparable to that available with the conventional (gasoline and diesel) fuels and engines.
e) Cost of operation similar to that of the conventional fuels (gasoline and diesel) and engines - preferably lower, to stimulate the initial market growth.
f) Operating savings or capital cost saving incentives to neutralize the additional initial vehicle costs and any other required conversion costs.
g) No impairment of carrying capacity, comfort, and safety.
h) The fuel must be non-toxic and should ideally generate as little exhaust emissions as possible.
i) The refueling process should be rapid and simple.

Some or all of these requirements are met in totality only by a few liquid fuels, very similar in performance and properties to that of gasoline and diesel. A few candidates for alternative fuels have emerged over the years, which appear to offer the best compromise among the key constraints of scale, availability, cost, and compatibility with the existing and the future vehicle infrastructure. Presently, the most promising alternative fuel candidates are compressed natural gas (CNG), liquefied petroleum gas (LPG) or propane, alcohols such as methanol and ethanol, and electricity.

The alternative fuels can primarily be grouped in three general categories: gaseous fuels, liquid fuels, and electricity, as shown in Table 1. While the gaseous and the liquid fuels can be combusted in internal combustion engines on board the vehicle, chemical energy stored inside a battery can be utilized to generate electrical energy to power an electric vehicle.

Table 1 Alternative fuel candidates

Gaseous Fuels	*Liquid Fuels*	*Electricity*
Methane (natural gas)	Reformulated gasoline and Bio-diesel	Battery
Propane (LPG)	Methanol	Fuel Cell
Hydrogen	Ethanol	

Among the three categories, the liquid fuels are the most compatible with the existing distribution systems and engines, as they require the least departure from the technologies in place today, for both the vehicles as well as the refueling infrastructure. On the other hand, fuels like methanol can prove detrimental to the fuel system because of its corrosive nature. Some liquid fuels, therefore, present another challenge related to the change in materials of some specific engine components, particularly the fuel system. Reformulated gasoline and reformulated diesel can also be considered as the alternative fuel candidates. The advantage with these fuels lies in the fact that they can be readily utilized because of the already available infrastructure. On the other hand the development of infrastructure for the other alternative fuels can be gradual and may not even be economically viable for some.

The third category of the alternative fuels, electricity, presents the most demanding challenges to the automobile industry, since the electric vehicle is the biggest departure from the vehicle technology in place today. The ultimate key to its success is breakthrough in battery technology.

1.2 Fuel Properties

Both physical and chemical properties as well as the combustion characteristics should be properly understood before recommending a particular fuel for its use in the internal combustion engines. Many of the inherent properties of a fuel such as the

calorific values (on both mass and volume basis), typical storage pressures and temperatures, and octane number ratings are quite different for the alternative fuels when compared to those of gasoline and diesel. Besides reducing dependency on the petroleum products, an equally significant objective is to be able to reduce vehicular emissions using these alternative fuels, without compromising the fuel efficiency and engine performance. Appendix 1 lists the significant fuel properties of all the various alternative fuel candidates, along with gasoline and diesel.

Natural gas and hydrogen can be stored on board the vehicle either as a highly pressurized gas, or as a liquid through cryogenic means. Storing these fuels in the liquid phase can be beneficial, as it reduces the space required for a given amount of energy. This, however, increases the cost and complexity of the system substantially. Gaseous fuels perform well in internal combustion engines, but their physical and chemical characteristics dictate that the engine be dedicated to the use of that fuel alone in order to achieve performance equivalent of gasoline. Hydrogen could also become an important fuel in the future, but for now it remains too expensive for its use in the internal combustion engines – about ten times the cost of gasoline per mile [**2**]. Its best use may be in fuel cell applications where good progress has been made in recent years, but this technology still remains very expensive and much research remains to be done.

1.3 Propane as an Alternative Fuel

Liquefied Petroleum Gas (LPG), mostly comprised of and commonly known as propane (C_3H_8), is one of the most popular and widely used alternative fuels in the world. Propane or LPG is a popular alternative fuel choice for vehicles, because there already is an infrastructure of pipelines, processing facilities, and storage for its efficient distribution. Besides being readily available, LPG produces fewer vehicular emissions than reformulated gasoline [**3**].

Propane is produced as a by-product of natural gas processing and crude oil refining. It offers potentially longer range as compared to CNG, because of its ability to be stored as a liquid at reasonably low pressures (0.0035-1.725 MPa) [**4**]. CNG is

usually stored at a higher pressure (2.7 MPa) and only as a gas. Also, there is a widespread network of LPG distributors and filling stations, which enable its widespread use. The composition of typical LPG is shown in Table 2.

Table 2 Composition of liquefied petroleum gas [**4**]

Fuel Component	*LPG Fuel Composition (volume percent)*
Propane (C_3H_8)	91.4
Propylene (C_3H_6)	6.1
Ethane (C_2H_6)	2.0
Butane (C_4H_{10})	0.4
Methane (CH_4)	0.1
Nitrogen (N_2)	0.0

Table 3 provides a comparison of LPG and iso-octane based upon the properties of each fuel. While the octane rating of propane is not quite as high as that of methane, it is still high enough (~112 RON) [**4**] to permit compression ratios of 10.5-11.1 with engines designed to operate on LPG. The engine should be dedicated to the use of propane in order to offset the inherent volumetric efficiency loss of gaseous fuel operation. The refueling infrastructure for propane is already quite extensive, with more than 5,000 stations across the nation.

Table 3 Comparison of selected properties of iso-octane and LPG [**4**]

Property	*Iso-octane*	*LPG*
Density, kg/L	0.75	0.51
LHV, MJ/kg	43.8	46.3
LHV, MJ/L	32.8	23.6
Typical Octane No.	95 RON 88 MON	112 RON 97 MON

LPG is derived from several different sources. It is typically extracted [**2**] from natural gas during its processing by virtue of their significantly different boiling points (-258 ° F for methane compared to -44 ° F for propane). When natural gas is produced, it consists of methane and other lighter hydrocarbons that are separated in a gas processing plant. Since, propane boils at -44°F and ethane boils at -127°F, it is separated from methane by the combined effect of increasing pressure and decreasing temperature at the same time. Propane is also produced in conjunction with crude-oil well refining and, therefore, is a by-product of refinery operations.

Propane fuelled vehicles generate fewer ozone-forming emissions than vehicles fuelled by the reformulated gasoline. In addition, tests on light-duty bi-fuel (propane and gasoline) vehicles have demonstrated a 98% reduction in the emissions of toxics such as benzene, 1, 3 butadiene, formaldehyde, and acetaldehyde, when the vehicles were fuelled using propane rather than gasoline [**3**].

2. OBJECTIVES AND MOTIVATION

The overall objective of this research project is to determine the difference between a propane-fuelled engine and an iso-octane-fuelled engine in terms of the engine performance and emissions characteristics, for the same engine geometry and operating conditions. The values of the engine performance parameters to be investigated will be determined using a thermodynamic cycle simulation of a four-stroke spark-ignition engine. The specific tasks to satisfy the primary objective are:

1. The first task is to extend the previous thermodynamic model to predict correct results for propane. The model was previously used to predict the emissions characteristics and engine performance parameters for iso-octane as the fuel. The extended model will be used to obtain results for both iso-octane and propane.

2. The second task is to conduct a comprehensive parametric study to investigate the effects of variations in engine design and operating parameters on engine performance, brake thermal efficiency, and nitric oxide (NO_x) emissions using propane as the alternative fuel, and compare the results with the corresponding results from iso-octane, for the same operating conditions and engine specifications. Some of these results from the simulation are expected to confirm the validity of the model.

3. The other important task is to include newer expressions for engine friction which more accurately predict the engine friction and also explicitly account for the oil viscosity. Friction mean effective pressure (fmep) is an input to the simulation program. The previous friction model was less elaborate and was based upon the friction data collected between 1980 and 1988 [**5**]. Recent engine data (e.g., improved oils, surface finish on piston liners, valve train mechanisms) suggested [**6**] that the model needed updating. The improved model is expected to give reasonable and more accurate

estimates of individual components and the total spark-ignition engine friction mean effective pressure.

The primary motivation behind this project was the availability of in-house data and some experimental results to validate the results from the simulation. Texas A&M University participated in the 1996 Propane Vehicle Challenge [**4**] finishing in the first place. The objective of that project was to convert an iso-octane-fuelled Chrysler minivan to a dedicated LPG-fuelled vehicle. Baseline vehicle testing was done at Texas A&M Riverside Campus, emissions testing was conducted at Southwest Research Institute in San Antonio, and the Engine Research Laboratory was utilized for engine testing. Thus, availability of in-house experimental data was one of the guiding factors for selecting the Chrysler minivan, 3.3 liter, V-6 engine for the present project.

3. LITERATURE REVIEW

A large amount of the previous work concerning propane as an alternative fuel, has been done primarily in the areas of design and development of its storage and injection techniques. Because of its relatively high octane number (RON =112), previous studies have tried to take advantage of this property, by redesigning the combustion chamber of the existing vehicles to increase the compression ratio. Series of student competitions such as the Propane Vehicle Challenge, sponsored in the past by the Department of Energy (DOE) in partnership with other sponsoring agencies, have been primarily aimed at studying the feasibility of propane as an alternative fuel. The primary objective of such competitions was to convert a gasoline fuelled vehicle to a dedicated propane operation, within certain limits of vehicle performance parameters similar to those for the gasoline-fuelled vehicle. The propane-fuelled vehicles had to meet the existing emission norms and safety codes. These projects predominantly entailed a conversion approach, which included activities such as, redesigning the combustion chamber or other engine modifications, sophisticated control systems, fuel storage and delivery. These design competitions essentially presented some practical challenges and, therefore, encouraged students to propose innovative solutions to the same, while using propane as an alternative fuel.

In short, relatively less research has been conducted in the areas of development and use of thermodynamic models, which have the capability to predict the engine performance parameters within reasonable limits of accuracy. Thermodynamic models have been developed in the past for spark-ignition engines, but fewer studies have indicated the use of these models for parametric studies using alternative fuels such as propane. Also, these limited parametric studies conducted in the past have been less comprehensive, and far from being conclusive for alternative fuels.

3.1 Previous Experimental Studies

The engine experiments from the previous studies [**7, 8, 9**] have determined both the engine-out exhaust hydrocarbon (HC) emissions, and the individual hydrocarbon species from single-cylinder tests. The results indicate that the total emissions and the individual species concentrations are influenced significantly by the chemical structure of the fuel. Unburned fuel constitutes a large fraction of the emitted hydrocarbons. On the other hand, NO_x emissions show a much smaller variation with the fuel structure. This latter observation for the gaseous fuels can be explained in part by the differences in their adiabatic flame temperatures and, in the case of liquid fuels, evaporative cooling of the intake charge during fuel injection.

Spark-ignition and compression-ignition engine combustion experiments [**7**] have been conducted using alternative fuels including propane. These experiments establish that flame extinction and high unburned hydrocarbon emissions result, when in-cylinder combustion temperatures fall below a critical threshold value of approximately 1920 K. Laminar flame computations were also completed for methane and propane to relate these experimentally determined limiting temperatures, to those associated with lean-limit conditions for sustained flame propagation under typical engine operating conditions. Laminar flame computations using numerical models for pressures above approximately 5.0 MPa predicted a lean limit at an equivalence ratio of 0.6 under normal operating conditions, where the adiabatic flame temperature was approximately 1900 K. These results reveal that at elevated pressures during combustion, the lean-limit product temperatures for these hydrocarbon fuels are considerably higher, and that these much higher temperatures will generate significant amounts of NO_x emissions.

These coupled studies (experimental and computational) indicate, that under conditions of high pressures in both spark-ignition and compression-ignition engines, high combustion temperatures are generated and relatively high NO_x formation rates is the inevitable result. Therefore, it may be impossible to reduce NO_x formation to very low levels if flame propagation at high temperatures are involved, and it will be

necessary to provide post-combustion after-treatment to reduce NO_x emissions to the legislated levels.

One of the experimental studies [**8**] was conducted to investigate the effect of fuel structure on emissions from spark-ignition engines. Tests were conducted on a single-cylinder engine at four operating conditions using alternative fuels including propane. Measurements of the emitted engine-out hydrocarbons, NO_x, carbon monoxide (CO), and carbon dioxide (CO_2) were made at each condition to examine the effects of flame temperature and hydrogen-to-carbon (H/C) ratio in the fuel. The percentage contribution of the unburned fuel to the hydrocarbon emissions was particularly attributed to the engine operating parameters, such as engine speed and spark timing. The baseline engine operating condition was at an equivalence ratio of (Φ=0.9), minimum advance before top-dead-center for best torque (MBT) spark timing, 1500 rpm, 90° C coolant temperature, and a load of 3.8 bar. These steady-state conditions are typical of mid-speed, mid-load engine operating conditions. In addition to the baseline testing, additional tests were conducted at 2500 rpm, MBT as -12° before top dead center (BTDC) spark advance, and Φ = 1.15, while other conditions were maintained same as the baseline. Spark sweeps were carried out for each fuel to determine the MBT spark timing.

The emitted mole fractions of NO_x for dried exhaust samples were determined for each engine operating condition. Methane showed the lowest NO_x levels among all the fuels used, reflecting the smaller nitrogen (N_2) fraction in the mixture, and a lower adiabatic flame temperature. The remaining fuels showed a slight increase in NO_x as the number of carbon atoms in the fuel molecules increased, although the difference was not very pronounced, consistent with the similar flame temperatures of these fuels. Iso-octane and iso-pentane emitted 15 % less NO_x than any other gaseous fuel except methane. These experimental studies suggested that fuel structure has a more profound effect on hydrocarbon emissions and CO emissions than on NO_x emissions. NO_x emissions showed a much smaller reduction, still significant (approximately 20%), variation with fuel structure. This observation may be primarily attributed to the

differences in adiabatic flame temperatures and, in the case of liquid fuels, evaporative cooling of the intake charge during fuel injection.

Small engine industry has also been active in recent years in exploring alternative fuels for their purpose. The primary object of one of the studies [**9**] was to quantify the improvements in emissions characteristics that could be obtained by using propane instead of gasoline. The other objective of that study [**9**] was to develop a carburetor that would aid in reducing the emissions from propane-fuelled engines. The test engine for the study was a single cylinder, 0.4 lit., overhead valve, air-cooled, four-stroke utility engine. Other than the fuel system, no significant modifications were made to the engine to accommodate the fuel being tested. A propane carburetor was developed which gave significantly improved emissions output. The results indicated that compared to gasoline, propane provides approximately a one-third reduction in the exhaust emissions and 14% better fuel economy. The engine produced 6% less power with propane carburetor. The study [**9**] also indicated that although propane can potentially lower emissions compared to iso-octane, some form of exhaust system after-treatment will always be required to meet the designated emission levels.

The propane fuel system provided 36% lower CO, 61% lower HC, 38% higher NO_x, and 45% lower (HC+ NO_x) than from the corresponding gasoline fuel system. The maximum brake horse power obtained from propane-fuelled engine was lower than that from the iso-octane-fuelled engine, which can be primarily attributed to the decreased volumetric efficiency for propane. The propane was introduced as a vapor into the carburetor, and it displaced more air than the liquid gasoline. Calculation of the volume of air displaced by propane predicted a drop in power by 4.5%. Gasoline, on the other hand, provides evaporative cooling of the intake air which increases the intake air density and increases volumetric efficiency and power. Test results revealed 6% less power with propane fuelled engine than with gasoline fuelled engine [**9**].

The study [**9**] also revealed a significant difference in NO_x between propane and iso-octane-fuelled engines at higher loads and air-fuel mixtures leaner than stoichiometric. At full and ¾ load, the engine produced 3 to 5 g/hp-hr of NO_x

(approximately 50% more NO_x) with propane than with iso-octane. Formation of NO_x is primarily a function of peak combustion temperature. The engine can run leaner with propane and still maintain good combustion. In case of iso-octane also, mixtures lean of stochiometric ($\Phi < 1$) may aid in reducing the peak combustion temperatures. But such lean mixtures may lead either to poor combustion or even flame extinction, which in turn would result in higher percentage of HC emissions. Also, the different heat of vaporization of the two fuels may have affected the NO_x formation rates. Iso-octane enters the combustion chamber at least partially as a liquid. The energy used to vaporize gasoline is no longer available to raise cylinder temperature, resulting in relatively lower peak combustion temperatures. Propane, however, already enters the combustion chamber in the vapor form, and therefore cannot take advantage of this phenomenon. This could be another possible reason for the difference in the peak combustion temperatures and the corresponding NO_x formation.

The above studies [**9**] have also suggested that a fuel system that brings propane into the carburetor or combustion chamber in liquid form could be beneficial. The fuel density would be greater due to the cooling effect, allowing better volumetric efficiency. The cooling effect of the vaporizing propane would help lower the peak combustion temperatures, thereby reducing NO_x formation.

Experiments were done [**10**] to conduct a parametric study to determine the performance of vapor and liquid propane injection in a spark-ignition multi-point port injected (MPI) engine. A six cylinder inline engine was used over a wide range of speeds and torques, while the air/fuel ratio, compression ratio, and the injection timing were all varied. Tests were conducted at the standard compression ratio of 9.65:1 with the original gasoline MPI system, propane vapor MPI, and single point throttle body propane vapor injection. Vapor and liquid propane MPI were then tested at a compression ratio of 11.7:1. The results showed significant differences in performance between vapor and liquid propane MPI injection, as well as the MPI and throttle body injection for gasoline. Results from the experiments suggested that the difference in the method of mixing can have a significant effect on the engine performance. Significant

improvements in performance parameters were achieved when compared to gasoline, particularly specific emissions reductions of 88% for HC, 45% for NO_x, 40% for CO_2, 92% for CO, and a rise of 27% in thermal efficiency. The results indicated that from the practical standpoint, LPG MPI, both liquid and vapor systems, coupled with increased compression ratio could deliver superior emissions characteristics, increased power, and comparable fuel economy (on volume basis) to gasoline.

3.2 Previous Computational Studies

Previous numerical simulations [**11**] of flow, heat release rate, and exhaust emission characteristics have been developed for single cylinder engines operating on propane as the fuel. The studies have established the effects of combustion chamber geometry and engine operating parameters on flame growth within the combustion chamber, to determine its effect on exhaust emission levels.

A zero-dimensional model was used in the past [**12**] to predict exhaust emissions, such as CO, CO_2, NO_x and hydrocarbons. The engine was fuelled with two alternative fuels; natural gas and propane. ZMOTTO, a zero-dimensional transient model of a four-stroke spark-ignition engine was used for the numerical analysis. The engine was simulated for different load conditions for both fuels under consideration. The model was run at two different levels of sophistication in the chemistry sub-model, namely, equilibrium and kinetic flame, both with post combustion finite rate chemistry. The experimental conditions were the same for methane and propane and the equivalence ratio was held constant. The propane-fuelled engine was a hypothetical situation, due to the lack of experimental data to support the simulated results for propane. The similarity of emission trends between propane and methane established some confidence in the model. More experimental data was required for validation of the model for propane.

Previous studies included one analytical study [**13**], aimed to investigate the factors influencing the heat losses in a propane-fuelled four-stroke spark ignition engine. A parametric study was conducted to determine the factors influencing heat losses, primarily during the expansion stroke. The effect of equivalence ratio, compression ratio, spark plug location, and combustion duration at different speeds on the heat losses was examined for wide open throttle (WOT) conditions.

3.2.1 Effect of Spark Timing

Advancing the spark timing causes an increase in the percentage of heat losses, because advancing the spark causes the combustion to be completed near the top dead center (TDC), hence, more time would be available for the combustion products to loose energy to the surroundings. The percentage heat loss increases as the mixture is enriched, reaching its peak at mixtures around stoichiometric (Φ = 0.8 to 1.0) because of the higher thermal energy released. This situation drastically changes at richer than stoichiometric (Φ > 1.0) mixtures because of the poor combustion [**13**].

3.2.2 Effect of Compression Ratio

Increasing the compression ratio increases the percentage heat losses due to the overall increase in the cylinder temperatures and the near TDC completion of combustion. Shifting the spark plug location from the edge towards the center reduces the percentage heat losses, as it reduces the flame travel path and hence reduces the combustion duration [**13**].

3.2.3 Effect of Engine Speed

As the engine speed is increased, the time available for the combustion to be completed or the products of combustion to impart some of its energy to the surroundings is reduced, causing lower heat losses [**13**].

3.2.4 Effect of Valve Opening Area

Increasing the valve opening area, either by increasing its diameter or its lift, has a favorable effect on reducing the heat losses. This is because of the availability of more fresh mixture trapped inside the cylinder. It is, however, recommended that the valve diameter be increased rather than the valve lift as increasing the valve lift makes the operation noisier [**13**].

3.2.5 Effect of Combustion Duration

Lengthening the combustion duration or lowering the flame speed causes an increase in the heat loss, since the products of combustion have more time to loose energy to the surroundings. This effect dominates at lower engine speed, perhaps due to lesser turbulence inside the cylinder [**13**].

3.3 Summary

As already stated earlier, fewer analytical studies have been conducted in the past which were primarily aimed at investigating the effects of variations in various engine parameters on engine performance and emissions characteristics, using propane as the alternative fuel. Experimental studies are both time consuming and extremely expensive. The analytical studies conducted in the past were either inconclusive or incomplete in the sense that very few parameters were studied.

There is a need for a more comprehensive study for the alternative fuels and its parallel comparison with the results obtained from isooctane. There is a need for a robust and a more detailed thermodynamic model, which can predict results for various alternative fuels within reasonable limits of uncertainty, just by switching from one fuel to the other through the input to the simulation program. The present research, however, aims to conduct a complete parametric study using only propane as the alternative fuel for its corresponding comparison with iso-octane. This parametric investigation will be more comprehensive than some of the previous studies. Effects of variations in load, engine speed, equivalence ratio, percentage exhaust gas recycle, combustion duration,

spark timing, and compression ratio will be conducted using propane as the alternative fuel and will be compared with those obtained for isooctane, for the same operating conditions and engine specifications. The engine performance parameters selected for the analysis are brake specific fuel consumption, mean exhaust temperature, and brake specific nitric oxide emissions.

4. SIMULATION DESCRIPTION

In the present study, a thermodynamic model also known as the zero-dimensional model of a conventional spark-ignition engine operating on the four-stroke cycle was used. The model is primarily based on the first law of thermodynamics. Nitric oxide emissions are calculated using the extended Zeldovich kinetic [**14**] scheme.

The inputs to the calculation are: engine geometry; engine speed (N); equivalence ratio (Φ); percentage exhaust gas recycle fraction (%EGR); intake manifold pressure (P_{in}) and temperature (T_{in}); and parameters which define the burning law. One dimensional quasi-steady flow models were used for the intake and the exhaust processes. The first law of thermodynamics is used to determine conditions in the engine cylinder during compression, combustion and expansion. Empirical correlations are used for heat transfer in conjunction with a simple boundary layer model.

The model or cycle simulation then predicts the following: mass flow rate through the engine, cylinder pressure, unburned and burned mixture temperatures, heat transfer to the combustion chamber walls, work transfer to the piston, all as functions of crank angle during the cycle; and the indicated power, specific fuel consumption, thermal efficiency, mean effective pressure and mean exhaust temperature at the selected operating point.

4.1 Model Description

The features which are critical in interpreting the model predictions are briefly presented in this section. The key areas are: Basic assumptions; Combustion model; Definitions; and Method of solution. A more detailed description may be found elsewhere [**15**].

4.1.1 Basic Assumptions

The following assumptions were made in developing the cycle simulation model for conventional spark-ignition engine:

1) The engine cylinder is treated as a variable volume plenum. The cylinder pressure is a function of time only.
2) The charge is assumed homogeneous during intake and compression. During combustion, three zones exist: an unburned zone, an adiabatic burned zone, and a boundary layer burned zone. Each zone is assumed to be uniform in composition and temperature.
3) The volume of gas where the fuel oxidation process occurs is assumed to be negligible.
4) It is assumed that the individual species in the gas mixture behave as ideal gases. The unburned gas is composed of a non-reacting mixture of air, fuel, and the residual gases. The burned gases are a mixture of reacting gases, assumed to be in chemical equilibrium.
5) Quasi-steady, adiabatic and one-dimensional flow equations are used to predict the mass flow past the valves.
6) The intake and exhaust manifolds are treated as infinite plenums having specified temperature and pressure histories. When reverse flow past the intake valve occurs, a plug flow model is assumed.
7) Heat transfer is predicted with the correlations of Woschni [**14**] developed for a compression-ignition engine and generally applied to the spark-ignition engines.
8) The mass fraction burned as a function of crank angle is specified by a Weibe function [**14**].
9) Nitric oxide emissions are calculated by using the extended Zeldovich kinetic scheme, with the steady state assumption for the N_2 concentration and the equilibrium values used for H, O_2, and OH concentrations in the adiabatic core. The sudden freezing assumption is used for calculating boundary layer NO. This assumes that the NO accompanying the mass transfer to the boundary layer is immediately frozen [**15**].

4.1.2 Combustion Model

A three zone combustion model is used to describe the combustion process. The use of three zones - two burned and one unburned – was dictated by the inclusion of heat transfer and NO_x formation calculations. The mass fraction of the charge within the cylinder which has burned at a given crank angle is specified by a Weibe function of the following form [**14**] shown in eq. (1).

$$x = 1 - e^{-a[(\theta-\theta_0)/\Delta\theta_b]^{m+1}} \quad (1)$$

where,

x = fraction of the total combusted mass in the cylinder

a = efficiency parameter

m = form factor

θ = crank angle

θ_o = start of combustion

$\Delta\theta_b$ = combustion duration

4.1.3 Definitions

The following definitions will be used repeatedly in discussing the simulation output. For convenience, definitions have been grouped together in this section.

i) Start of Combustion (θ_o)

The crank angle corresponding to the start of combustion (θ_o) needs to be specified as an input. For $\theta>\theta_o$, the mass fraction burned is given by the Weibe function, eq. (1). The start of combustion is related to the spark timing by an ignition delay ($\Delta\theta_{id} = \theta_o - \theta_s$, where θ_s is the spark timing), as shown in the Figure 1.

ii) Combustion Duration ($\Delta\theta_b$)

The combustion duration ($\Delta\theta_b$) is specified as an input. This is the crank angle interval from start of combustion to the 100 percent burned position of the curve in Figure 1.

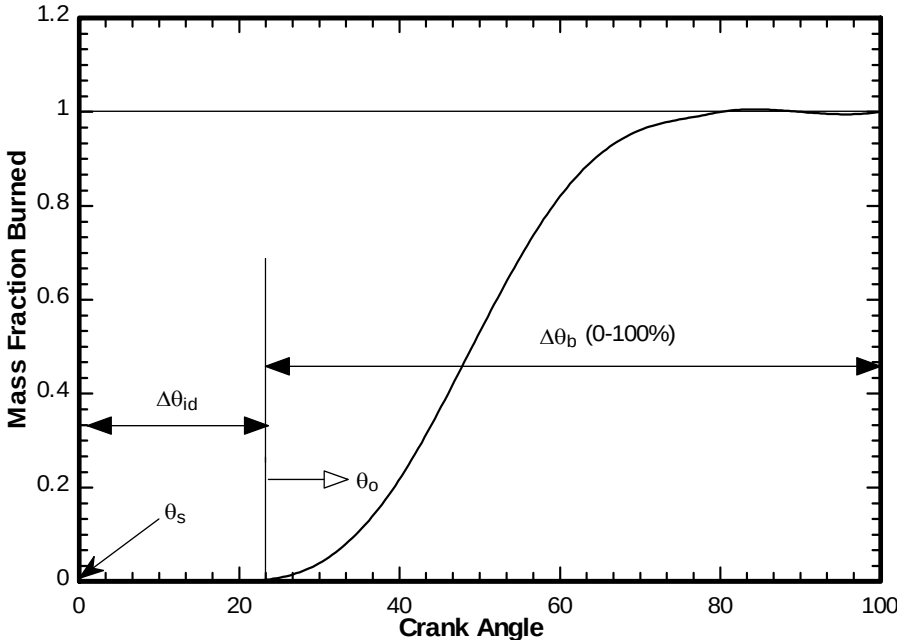

Fig. 1 Schematic of mass fraction burned profile [**15**] (Redrawn)

iii) Indicated Performance and Emissions Parameters

The conventional definition of indicated mean effective pressure (imep) is used; i.e., the values are computed by integrating over the compression and the expansion strokes of the four-stroke cycle. In parametric studies where load is held constant, it is brake mean effective pressure (bmep) which is fixed in value. Total friction mean effective pressure is computed for different inlet pressure conditions, compression ratios and engine speeds.

iv) Mean Exhaust Temperature (T_{exh})

For each calculation, a mean exhaust temperature is computed by interpolation from the following equation [**15**]:

$$\bar{h}_{exh}(\bar{T}_{exh}, P_{exh}) = \int_{\theta_{EVO}}^{\theta_{EVC}} \dot{m}\, h_{ev} \frac{d\theta}{360N} \Big/ \int_{\theta_{EVO}}^{\theta_{EVC}} \dot{m} \frac{d\theta}{360N} \qquad (2)$$

where,

$\dot{m}$ = instantaneous mass flow through the exhaust valve

$\bar{h}_{exh}$ = mass average enthalpy at exhaust

p_{exh} = exhaust manifold pressure

h_{ev} = instantaneous enthalpy of gases exiting the cylinder

N = engine speed

The calculated values of T_{exh} may be higher than the typical measured exhaust gas temperatures because heat losses to the exhaust valve, in the exhaust port and in the exhaust manifold, during the exhaust process are not included in the computed value [**15**].

4.1.4 Method of Solution

The basic simultaneous differential equations which need to be integrated to simulate the engine cycle are [**15**]:

A) Gas Exchange and Compression Processes

i) Energy conservation for the cylinder contents.

ii) Mass flow rate equations for intake and exhaust valves.

iii)Woschni's correlation for the heat transfer to the walls.

B) Combustion and Expansion Processes

i) Energy conservation equations for unburned adiabatic core and boundary layer systems.
ii) Mass burn rate equation.
iii) Woschni's correlation for heat transfer to the walls for burned and unburned systems.
iv) Equations for the rate of change of the mass of nitric oxide in the adiabatic core and boundary layers.

These equations are solved using a modified Euler predictor-corrector technique [**15**]. This integration scheme is adequate for solving a system of thermodynamic equations. The NO_x equations are solved using a fourth order predictor-corrector scheme. This added complexity is necessary for accurate integration of the governing equation for NO_x, since the NO_x kinetics is extremely temperature dependent.

4.2 Extension of Thermodynamic Model

One of the tasks as stated earlier was to extend the previous thermodynamic model to predict engine performance parameters and other results for propane as the alternative fuel. To satisfy this objective, the calorific value of propane was included along with the previously used calorific value of iso-octane. The chemical composition of propane is C_3H_8 while that of iso-octane is C_8H_{18}. The stochiometric equation and the fuel composition needed to be changed to accommodate propane.

4.2.1 Improved Friction Relations

Friction mean effective pressure (fmep) is one of the input parameters in the simulation model, and it required updating to accurately predict the complete engine friction. The previous model was based on the engine friction data collected between 1980 and 1988 [**5**]. Modifications were required to be made to the piston ring tension and gas pressure loading terms, the impact of liner roughness, and to the valvetrain

mechanism friction. Lubricant viscosity scaling was added to the hydrodynamic terms in the rubbing friction component models. The improved model [**6**] now gives reasonable estimates of individual friction components and total spark-ignition engine friction mean effective pressure.

A) Component Breakdown

Engine friction losses are typically divided into three main categories: mechanical or rubbing losses, pumping losses, and auxiliary component losses.

i) Mechanical friction can be divided into three component groups,

1. Crankshaft - main bearings, front and rear main bearing oil seals.
2. Reciprocating – connecting rod bearings, piston skirts, and piston rings.
3. Valvetrain – camshafts, cam followers, and valve actuation mechanisms.

ii) Auxiliary Losses

oil pump, water pump, and alternator.

iii) Pumping Losses

intake system, intake and exhaust ports and valves, and exhaust system.

B) Incorporating Lubricant Viscosity

The hydrodynamic terms in the Patton et al. [**5**] model needed to be modified to account for the differences between engine oil grades and the temperature dependence of oil viscosity. The tribilogy literature [**16**] shows that the viscosity scaling in the hydrodynamic friction terms should have the form

$$\mu_{scaling} = \sqrt{\frac{\mu(T)}{\mu_o(T_o)}} \tag{3}$$

where, $\mu(T)$ is the viscosity of the oil in the engine for which friction predictions are being made, and $\mu_o(T_o)$ is the reference viscosity for the oil used in the engines that provided the data used to calibrate the model when it was originally developed.

Since the relationship between υ and μ is the lubricant density, which is essentially constant, the above equation can be written as

$$\mu_{scaling} = \sqrt{\frac{\upsilon(T)}{\upsilon_o(T_o)}} \tag{4}$$

where, $\upsilon(T)$ is the kinematic viscosity of the oil in the engine that is being tested, and $\upsilon_o(T_o)$ is the reference viscosity at the reference temperature T_o.

The Vogel equation, which relates oil temperature and low shear kinematic viscosity was used in the form

$$\upsilon_o = k \,.\, \exp\left(\frac{\theta_1}{\theta_2 + T}\right) \tag{5}$$

where, υ_o is the low shear rate viscosity of the oil, and k, θ_1, and θ_2 are the correlation constants for an oil and T is the oil temperature in ° C. The low shear rate viscosity υ_o was then multiplied by a ratio (μ_∞/μ_o) to convert to the high shear rate kinematic viscosity used in the model. This was done because most of the engine components operate in the high shear range where multi-grade oils exhibit shear thinning. Thus,

$$\upsilon = \upsilon_o\left(\frac{\mu_\infty}{\mu_o}\right) \tag{6}$$

Viscosity data for several oil grades, and the constants used in eqs. (5) and (6) are listed in Appendix 2.

C) Modifications

This section presents the expressions previously used for predicting friction values, followed by the modified expressions for the same for each individual friction component.

i) Mechanical Fiction

1. Crank Shaft Friction

In the Patton et al. [**5**] model, crankshaft friction mean effective pressure (cfmep) was estimated by adding a term representing front and rear main bearing seal friction, to the terms representing the main bearing friction. The main bearing friction terms included a hydrodynamic journal bearing term and a turbulent dissipation term, the latter accounting for losses due to the transport of oil through the bearings. The three terms that made up the crankshaft friction were:

$$\text{cfmep}_{\text{old}} = 1.22\times10^{5}\left(\frac{D_b}{B^2 S n_c}\right) + 3.03\times10^{-4}\times\left(\frac{N D_b{}^3 L_b n_b}{B^2 S n_c}\right) + 1.35\times10^{-10}\left(\frac{D_b{}^2 N^2 n_b}{n_c}\right) \tag{7}$$

The first term gave the friction of the main bearing seals. The seals were assumed to operate in the boundary lubrication regime due to direct contact between the seal lips and the crankshaft. The seal lip load was assumed to remain constant. The second term was for the main bearing hydrodynamic lubrication friction, derived using the friction coefficient for hydrodynamic lubrication. The last term accounted for the turbulent dissipation, the work required to pump fluids through flow restrictions.

Modifications:

The only modification made to the crankshaft friction model was to include the viscosity scaling $\sqrt{\frac{\mu}{\mu_o}}$ in the hydrodynamic friction term:

$$\text{cfmep}_{\text{new}} = 1.22\times10^{5}\left(\frac{D_b}{B^2 S n_c}\right) + 3.03\times10^{-4}\times\sqrt{\frac{\mu}{\mu_o}}\left(\frac{N D_b{}^3 L_b n_b}{B^2 S n_c}\right) + 1.35\times10^{-10}\left(\frac{D_b{}^2 N^2 n_b}{n_c}\right) \quad (8)$$

2. Reciprocating Friction

The equation for the reciprocating component of mechanical friction in the Patton et al. [**5**] model included piston skirt, piston ring, and connecting rod friction. Piston ring friction was divided into two terms; one that predicted friction for the piston rings without gas pressure loading, and the other that predicted the increase in piston ring friction caused by the gas pressure loading. The resulting reciprocating friction mean effective pressure (rfmep) equations were:

Terms without gas pressure loading:

$$\text{rfmep}_{\text{old}} = 2.94\times10^{2}\left(\frac{S_p}{B}\right) + 4.06\times10^{4}\left(1+\frac{1000}{N}\right)\left(\frac{1}{B^2}\right) + 3.03\times10^{-4}\left(\frac{N D_b{}^3 L_b n_b}{B^2 S n_c}\right) \quad (9)$$

The first term gives the piston friction assuming hydrodynamic lubrication. The second term is for the piston ring friction under mixed lubrication. The function, (1+1000/N), was used to make the friction coefficient decrease by a factor of 2.5 as the

engine speed range changes from low to high speeds. The last term accounts for the hydrodynamic journal bearing friction from the connecting rod bearings.

Terms with gas pressure loading:

$$\text{rfmep}_{\text{gasold}} = 6.89\frac{p_i}{p_a}\left[0.088r_c + 0.182r_c^{(1.33-KS_p)}\right] \tag{10}$$

The term for piston ring friction due to gas pressure loading used the product of intake pressure (p_i) and a factor which included the compression ratio (r_c) and mean piston speed (S_p), derived from the physics of the compression process.

Modifications:

Several modifications were made to the piston terms, as there have been improvements in the piston ring and liner details which have reduced the friction between these two surfaces.

Terms without gas pressure loading:

$$\begin{aligned}\text{rfmep}_{\text{new}} = {} & 2.94\times10^{2}\sqrt{\frac{\mu}{\mu_o}}\left(\frac{S_p}{B}\right) + 4.06\times10^{4}\left(\frac{F_t}{F_{to}}C_r\right)\left(1+\frac{500}{N}\right)\left(\frac{1}{B^2}\right) + \\ & 3.03\times10^{-4}\left(\frac{ND_b{}^3L_bn_b}{B^2Sn_c}\right)\end{aligned} \tag{11}$$

For the equation without gas pressure loading, the viscosity scaling was incorporated into the piston friction and connecting-rod bearing hydrodynamic terms. For the piston ring friction term, three modifications were made. Two factors, piston ring tension and surface roughness, were included to take into account the reductions in piston friction that have occurred in these areas. The final change was to decrease the

value of the function (1+1000/N) to (1+500/N) to make the friction coefficient decrease by a factor of 1.8 instead of 2.5. Experimental data indicated that the boundary lubrication contribution to the friction coefficient has reduced.

Terms with gas pressure loading:

$$\text{rfmep}_{\text{gasnew}} = 6.89\frac{p_i}{p_a}\left[0.088\sqrt{\frac{\mu}{\mu_o}}r_c + 0.182\left(\frac{F_t}{F_{to}}\right)r_c^{(1.33-2KS_p)}\right] \tag{12}$$

Viscosity scaling was included in the first term. In the second term, the piston ring tension factor was included. For the exponential term, the constant K was doubled to 2.8×10^{-2} to reflect a reduction in piston liner roughness.

3. Valvetrain Friction

The original valvetrain component friction equation included the estimates of camshaft, cam follower, and valve actuation mechanism friction for a variety of valvetrain configurations. The model needed to be able to predict friction for all the common types of valve configurations. Individual terms in the equation modeled camshaft bearing hydrodynamic friction, cam follower friction, and oscillating mixed lubrication. The resulting expression was,

$$\begin{aligned}\text{vfmep}_{\text{old}} = {} & 244\frac{Nn_b}{B^2Sn_c} + C_{ff}\left(1+\frac{1000}{N}\right)\frac{n_v}{Sn_c} + C_{rf}\left(\frac{Nn_v}{Sn_c}\right) + \\ & C_{oh}\left(\frac{L_v^{1.5}N^{0.5}n_v}{BSn_c}\right) + C_{om}\left(1+\frac{1000}{N}\right)\frac{L_vN_v}{Sn_c} + 4.12\end{aligned} \tag{13}$$

The first term represents the camshaft bearing hydrodynamic friction, with a form similar to the main and connecting rod journal bearing terms. The next two terms predicted friction resulting from relative motion between the cam lobe and the cam

follower. The second term predicted friction in the mixed lubrication regime for flat follower configurations. The third term predicted rolling contact friction for roller follower configurations. The fourth term, oscillating hydrodynamic friction predicts friction caused by the relative motion between valvetrain components whose lubrication states were either completely or partially hydrodynamic, such as the valve lifter in the lifter bore or the valve in the valve guide. The fifth term represents mixed lubrication friction contribution. Experimentally determined engine data indicated that some of the valvetrain friction was independent of the piston speed, and a constant 4.12 kPa was added to represent the boundary-lubricated friction from the camshaft bearing seals. The constants for the valvetrain terms (C_{ff}, C_{rf}, C_{oh}, and C_{om}) were dependent on the type of valvetrain configuration being modeled.

Modifications:

Two modifications were made to the valvetrain friction terms. The first was to include the viscosity scaling in the camshaft bearing and oscillating hydrodynamic friction terms. The second was to lower the value of the function (1+1000/N) to (1+500/N) in the flat follower and oscillating mixed lubrication terms.

$$\begin{aligned} \text{vfmep}_{\text{new}} = 244\sqrt{\frac{\mu}{\mu_o}}\frac{Nn_b}{B^2Sn_c} + C_{ff}\left(1+\frac{500}{N}\right)\frac{n_v}{Sn_c} + C_{rf}\left(\frac{Nn_v}{Sn_c}\right) + \\ C_{oh}\sqrt{\frac{\mu}{\mu_o}}\left(\frac{L_v{}^{1.5}N^{0.5}n_v}{BSn_c}\right) + C_{om}\left(1+\frac{500}{N}\right)\frac{L_v n_v}{Sn_c} + 4.12 \end{aligned} \tag{14}$$

ii) Auxiliary Friction

The auxiliary friction component was an empirical match to the sum of oil pump, water pump, and non-charging alternator friction mean effective pressure. The resulting expression for auxiliary friction mean effective pressure (afmep) was

$$\text{afmep}_{\text{old}} = 6.23 + 5.22\times10^{-3}\,\text{N} - 1.79\times10^{-1}\,\text{N}^2 \tag{15}$$

Modifications:

The original model increasingly under predicted auxiliary friction above an engine speed of approximately 3000 rpm. The equation for afmep was recalibrated to fit the newer engine data.

$$\text{afmep}_{\text{new}} = 8.23 + 1.86\times10^{-3}\,\text{N} + 7.45\times10^{-7}\,\text{N}^2 \tag{16}$$

iii) Pumping Losses

The original pumping loss model predicted intake and exhaust pumping mean effective pressures (pmep), each defined as the difference between cylinder pressure and atmospheric pressure integrated over the volume of the intake or exhaust stroke. The intake and exhaust terms were:

Intake

$$\text{pmep}_{\text{in}} = (\text{p}_\text{a} - \text{p}_\text{i}) + 4.12\times10^{-3}\left(\frac{\text{p}_\text{i}}{\text{p}_\text{a}}\right)^2\left(\frac{\text{S}_\text{p}^{\,2}}{\text{n}_\text{v}^{\,2}\,\text{r}_\text{i}^{\,4}}\right) \tag{17}$$

The first term is the intake manifold vaccum, calculated as the difference between atmospheric and the intake pressure. The second term predicted the intake port and valve pressure drop.

Exhaust

$$\text{pmep}_{ex} = 0.178\left(\frac{p_i}{p_a}S_p\right)^2 + 4.12\times10^{-3}\left(\frac{p_i}{p_a}\right)^2\left(\frac{S_p{}^2}{n_v{}^2 r_e{}^4}\right) \qquad (18)$$

The first term estimates the exhaust system pressure drop, derived from measurements from typical production engine systems. The second term represents the exhaust valve and port pressure drop.

Modifications:

In the modified model, the constant for the valve pressure drop was changed to 3.0×10^{-3} kPa - s^2/m^2, following Patton's suggestion [**5**]. The smaller constant also takes into account improvements in intake manifold and cylinder head design. With this change, the model gives more accurate predictions of the intake and exhaust pressure losses.

This completes the updating of friction expressions. The improved model now gives lower and more accurate estimates of individual friction components and total spark-ignition engine friction mean effective pressure. The effect of improved model due to gas loading effect and other modifications is illustrated in Appendix 3.

5. EXPERIMENTAL BACKGROUND

One of the motivations for choosing this project was the availability of in-house data and experimental results to validate the model. This was the primary reason for choosing 3.3 liter, V 6, Chrysler Minivan engine for this study. Texas A&M University participated and finished in first place in 1996 Propane Vehicle Challenge. Senior-level mechanical engineering students at Texas A&M University approached the 1996 Propane Vehicle Challenge in the context of a two-semester design project. The objective of the project was to convert the existing iso-octane-fuelled 3.3 liter, V-6, Chrysler Minivan, to a dedicated LPG fuelled vehicle.

5.1 Conversion Methodology

Five major task areas were identified as critical to a successful design. This determination was based on a functional breakdown of the vehicle into systems significant in the conversion process. These areas included fuel storage, fuel delivery, engine development, exhaust and emissions, and electronics and controls. The following sections describe the designs developed for each of the five main subsystems.

5.1.1 Fuel Storage Design

The primary need of the fuel storage team was to safely store a sufficient volume of LPG fuel. The main constraint was the available space provided by the undercarriage of the 1996 Chrysler minivan. Two independently-mounted bi-manifold tanks were chosen in order to maximize the space available under the van without compromising safety. In addition, this bi-manifold design would prevent a complete loss of fuel in the event of leakage in one of the tanks. The two tank units were placed underneath the vehicle and were attached directly to the side rails by rubber isolated L-bracket mounting assemblies. The tanks featured in-line manual shut-off valves as well as an automatic shut-off valve operated electronically by the ignition switch. Other safety features

included an internal relief valve that would release tank pressure above the design pressure of 2.16 MPa.

5.1.2 Fuel Delivery System Design

The primary need of the fuel delivery system design was to collect the fuel from the storage tanks and deliver this fuel to the engine in adequate quantities. The primary constraint involved maintaining the desired phase of LPG throughout the delivery and the intake process. A sequential vapor injection scheme was considered most appropriate to satisfy the above objective. Vapor injection while sacrificing some performance due to the displacement of intake air, does not suffer from some of the drawbacks associated with liquid injection. LPG injected in liquid phase although would take up much less volume than an equivalent mass of LPG injected in the vapor phase, it requires relatively higher pressure (1.275 MPa) in the fuel system to maintain the fuel in the liquid state. Other advantages include lower operating pressures, reduced temperature constraints, and fewer or simpler mechanical components.

5.1.3 Engine Development Design

The primary goal of the engine development was to efficiently convert the energy of LPG to mechanical energy. The constraint to accomplish this task was without any modification to the engine block. Raising the compression ratio to theoretically increase the thermal efficiency appeared to be the appropriate choice. Also, it was a safe choice from knock perspective due to propane's high octane number (RON=112). New pistons were designed to decrease the clearance volume and increase the compression ratio. The compression ratio was increased from the existing value of 8.9:1 to a new value of 11.7:1. Optimal spark plugs were specified for the modified LPG engine, using heat range and spark plug gap as primary considerations. Several engine parts including the plenum, intake manifold, and exhaust manifold were polished, which resulted in increased air flow through these components. Additional friction reducing processes were applied to the engine bearings and exhaust manifold.

5.1.4 Exhaust and Emissions Design

The primary constraint in this design was meeting the rigorous 1997 California Ultra Low Emission Vehicle (ULEV) emission standards. Approximately more than 90% of the total emissions during a standard EPA FTP-75 emissions test occur during cold-start (first five minutes or bag one) conditions. A catalytic converter system with the shortest possible light-off time was selected. An electrically heated three-way catalyst (EHC), attached to a main catalytic converter was chosen, which used a resistive heating element to supply heat to the catalyst and reduce the light-off time.

After the catalyst system, the exhaust was routed outside the frame rails, returning in the vicinity of the last tank, which was designed to allow the necessary space for the exhaust routing. The system was designed for ease of assembly and low exhaust back pressure.

5.1.5 Electronics and Control Design

The primary task involved in electronics and control design was to sense the operating conditions of the vehicle, process these signals, and generate the outputs needed to implement the desired operating state. A MESA Environmental Gas Engine Management (GEM_{TM}) system was selected for this application. This system consisted of a GEM unit which controlled fuel metering, a timing interface module which adjusted ignition timing, and the original equipment manufacturer (OEM) unit. The GEM system was equipped to operate with a narrow-band closed loop oxygen sensor. This control system resulted in consistent stoichiometric operation, which maximized engine and catalytic converter efficiency. The controller also had an adaptive learning feature, which allowed the controller to monitor the exhaust over time and analyze the differences between the desired and actual operation of the engine. Upon detecting differences, the controller would adjust the system over time to maintain optimal calibration for all operating conditions.

While the engine was operating on the dynamometer, fuel calibrations were made utilizing the closed loop function of the controller. By reading the level of the

closed loop corrections necessary for stoichiometric operation, the correct calibration could be entered.

5.2 Testing

Extensive testing was conducted to evaluate the LPG-fuelled vehicle, and to compare its operating characteristics with those provided by the iso-octane-fuelled vehicle.

5.2.1 Baseline Vehicle Testing

Tests were conducted to evaluate the acceleration performance (0 – 60 mph time, quarter mile time and speed), braking performance (30 – 0 mph distance, 70 – 0 mph distance), and emissions.

5.2.2 Baseline Emissions Testing

The vehicle was taken to Southwest Research Institute in San Antonio, Texas for baseline emissions testing. A standard Federal Test Procedure emissions test (FTP-75) was completed for the iso-octane vehicle. While emissions testing were being completed, exhaust temperature and pressure measurements were made to gain an understanding of the stock exhaust system operation.

5.2.3 Engine Testing Methodology

Three engine and fuel system configurations were tested at various stages of the conversion process. Tests were conducted to determine the engine performance, thermal efficiency, and emissions characteristics and to obtain comparisons between each engine configuration. Table 4 illustrates the differences between each of the three engine testing configurations.

Table 4 Engine test configurations [**4**]

Stock Gasoline Engine	*Stock LPG Engine*	*Modified LPG Engine*
SFI Gasoline Injection	SFI LPG Vapor Injection	SFI LPG Vapor Injection
8.9:1 Compression Ratio	8.9:1 Compression Ratio	11:7 Compression Ratio
Stock Intake System	Stock Intake System	Polished Intake System
Stock Exhaust Manifold	Stock Exhaust Manifold	Polished and Coated Exhaust Manifold
Stock Components	Stock Components	Balanced Components
Stock Bearings	Stock Bearings	Friction Coated Bearings

5.2.4 Engine Testing Setup

The engines were mounted on a General Electric model TLC-50 dynamometer with a General Electric model CR1420 control and operation panel. The dynamometer was limited to 150 horsepower at 4000 RPM, so data was taken at or below this operating point.

For LPG operation, the GEM engine control unit and timing interface module were incorporated into the controls and wiring system.

5.2.5 Data Acquisition

Instrumentation was installed to acquire data for calculation of the performance, efficiency, and emissions characteristics of each engine configuration. Engine load was measured with a load cell attached to the dynamometer. Engine speed was recorded with a tachometer which measured the speed of the dynamometer input shaft. Throttle

position was measured from the throttle position sensor signal. Flow meters were attached to the fuel lines to measure the mass flow rate of fuel. Emissions equipment, including a NO_x analyzer and HC/CO analyzer, was used to determine engine-out hydrocarbon, carbon monoxide, and nitrogen oxide emissions.

5.3 Evaluation: Validation of the Model

As previously documented, the primary motivation for selecting 3.3 liter, V6, Chrysler Minivan engine was the availability of experimental data to confirm the validity of the simulation model. The details of the simulation model and the computations will be provided in section 6. This section aims to compare the experimentally determined engine performance parameters such as the brake torque and brake power with the corresponding simulated results at the same operating conditions which were maintained during the experiments. The comparison will be made using both the absolute values as well as their corresponding percentage relative differences. The percentage relative difference between the simulated and the experimentally determined brake torque and brake power is defined as:

$$\text{Percentage Relative Difference (Torque)} = \frac{T_{\text{simulated}} - T_{\text{experimental}}}{T_{\text{experimental}}} \times 100 \qquad (19)$$

$$\text{Percentage Relative Difference (Power)} = \frac{P_{\text{simulated}} - P_{\text{experimental}}}{P_{\text{experimental}}} \times 100 \qquad (20)$$

The negative values of the percentage relative difference would indicate that the simulated values are lower than the corresponding experimental values. The positive values, on the other hand, would indicate that the values for the experimental results are lower than the corresponding simulated values. The values (both negative and positive) nearer to zero would indicate high degree of correlation between the simulated results and the experimental values.

5.3.1 Engine Performance

Figure 2 shows the plots of brake torque and brake power as functions of engine speed for the stock iso-octane fuelled engine. As documented earlier, the stock engine had a compression ratio of 8.9:1. The figure includes plots generated from both the experimentally determined values as well as the values computed through the simulation. While Figure 2 shows the absolute values, Figure 3 shows the relative difference between the simulated and the experimental values.

The operating conditions during the experiments for these particular sets of plots were 100% WOT and the engine speed was varied from 1000 to 4000 rpm. Other operating conditions and engine performance parameters during the experiments were not documented in the literature. In the simulations, inlet manifold pressure (P_{in} = 90 kPa) was used to simulate 100 % WOT conditions.

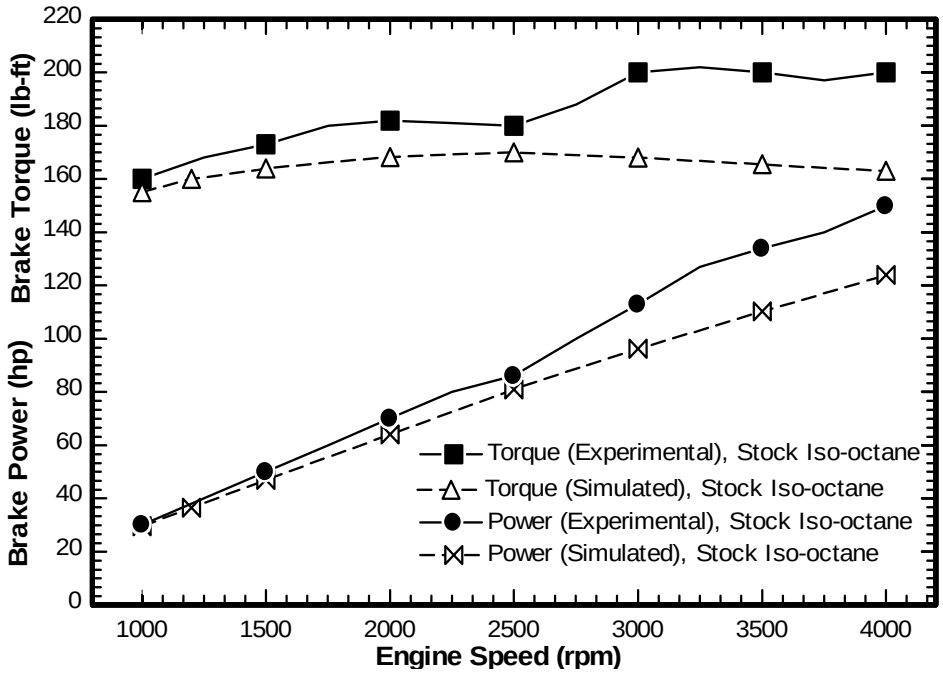

Fig. 2 Brake torque and brake horse power curves with the engine speed for 100% WOT condition for the stock iso-octane-fuelled engine

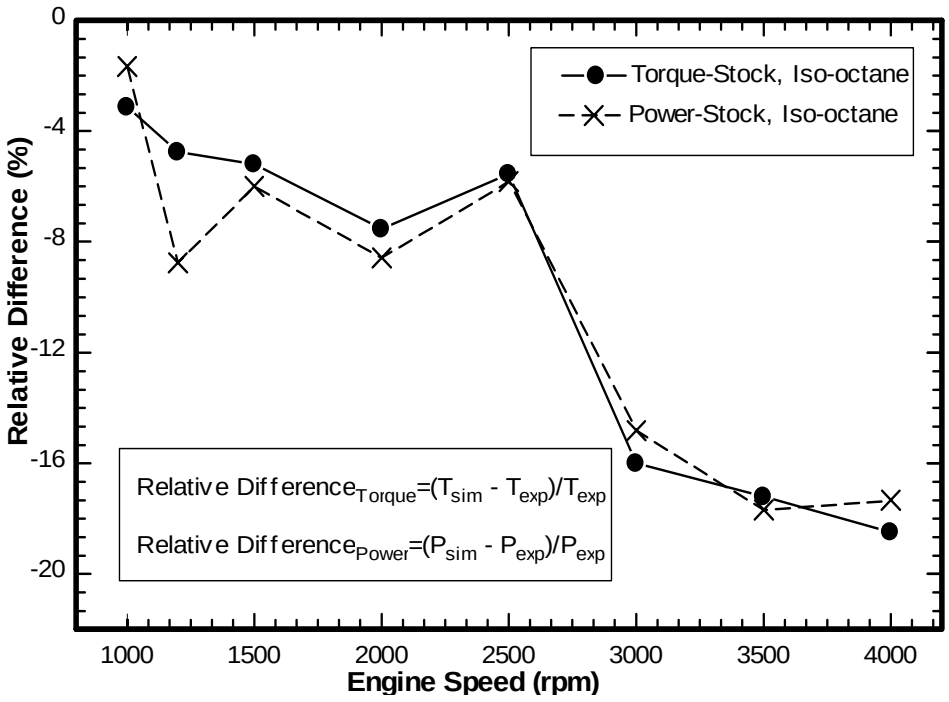

Fig. 3 Plots of percentage relative difference for brake torque and brake power with the engine speed for the stock iso-octane-fuelled engine

The simulated values of brake torque are lower than the experimentally determined values. This difference becomes more prominent in the high rpm range (2500 to 4000 rpm). In the low engine speed range (1000 to 2500 rpm), both simulated and the experimentally determined brake torque curves follow similar trends.

The difference between the simulated and the experimentally determined torque values can be attributed to a number of factors. One possible explanation is that the combustion durations and the MBT spark timings for the experimentally determined values could be different than the ones used in the simulation. As stated previously, the only operating conditions known from the literature were load and the engine speed. In the simulation, combustion duration of 60° was used while the MBT spark timing was advanced from - 36° BTDC to - 44° BTDC and the engine speed was increased from 1000 to 4000 rpm. Combustion duration of approximately 60° is representative of the typical engine operating conditions and therefore the same was considered for the

present simulation. Also, the dynamic flow effects due to the variation in engine speed have not been included in the simulation model, which might explain the increased difference between the simulated and the experimentally determined values in the higher engine speed range. Finally, the uncertainty in the experimentally determined values may account for the remaining difference.

The simulated values of brake power are approximately the same as the experimental values in the low engine speed range (1000 to 4000 rpm). Both the experimental and the simulated brake power curves follow similar trends. Power directly scales with the engine speed, and therefore the simulation predicts values closer to the experimental values. In the higher engine speed range (2500 to 4000 rpm), the difference between the simulated and experimental power increases due to the corresponding increase in the brake torque values.

Figure 4 shows the brake torque and brake power curves for the stock propane fuelled engine. The figure includes plots generated from both simulated and the experimentally determined values. The operating conditions for these plots were the same as for the experiments conducted on the stock iso-octane fuelled engine. Both the simulated brake torque and brake power curves follow trends similar to the plots generated from the experimentally determined values. Also, the magnitudes of the brake torque and brake power are approximately the same in the low engine speed range (1000 to 2500 rpm).

In the high engine speed range (2800 to 4000 rpm), the simulated values of brake torque and brake power are lower than the corresponding experimentally determined values. The explanation for this observation could be the difference in burn durations and spark timings used in the simulation and the actual experiments.

While Figure 4 shows the absolute values of brake torque and brake power, Figure 5 shows the corresponding relative difference for the stock propane engine.

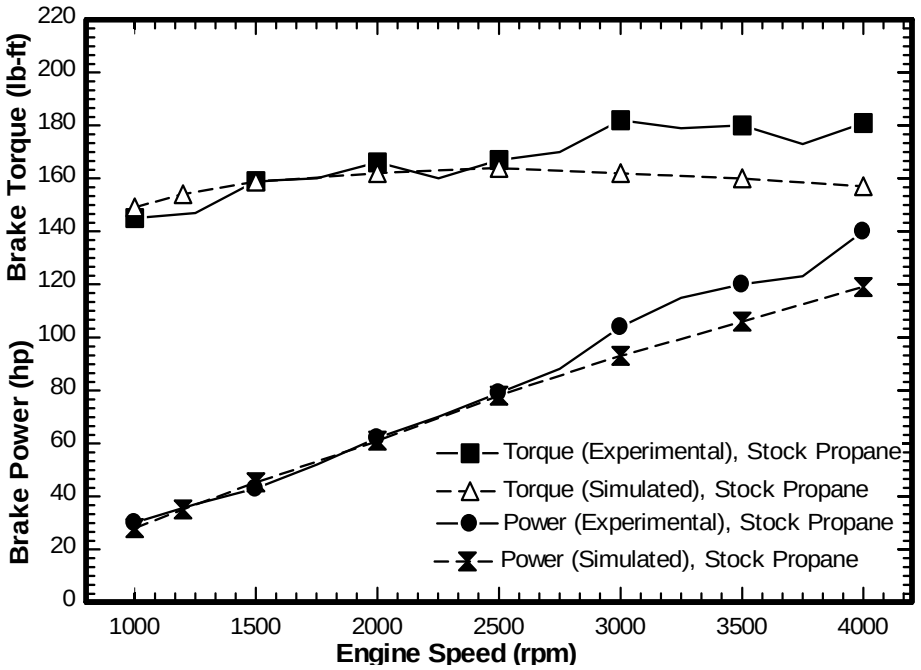

Fig. 4 Brake torque and brake horse power curves with the engine speed for 100% WOT condition for the stock propane-fuelled engine

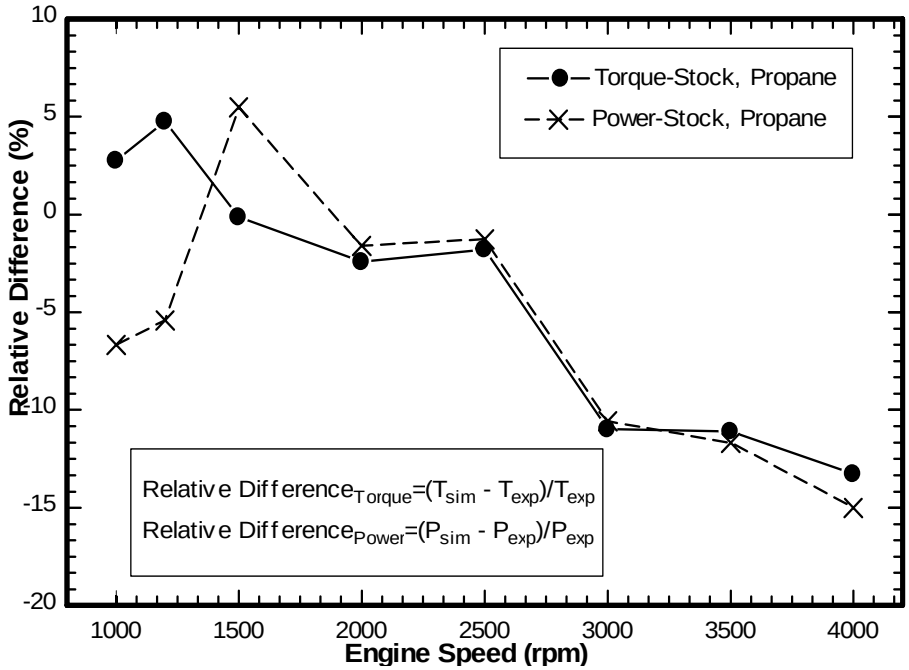

Fig. 5 Plots of percentage relative difference for brake torque and brake power with the engine speed for the stock propane-fuelled engine

Figure 6 presents the brake torque and brake horse power curves with engine speed using both simulated and the experimentally determined values for the modified propane fuelled engine. As observed in the previous case for the stock engine, once again the brake torque and brake horse power curves show acceptable similarity in terms of the trends and the magnitudes obtained from the experiments for the engine speed range below 3000 rpm. The difference in the simulated and the experimentally determined values can be attributed to the combustion duration values being possibly different for the two cases. For a compression ratio of 11.7 (raised from 8.9) for the modified engine, the MBT spark timing was required to be adjusted accordingly in the simulation because the spark timing is a function of compression ratio also. The MBT spark timing was now varied from - 40° BTDC to - 48° BTDC. Again the actual MBT spark timing might be different from the ones used in the simulation and might have resulted in different brake torque values.

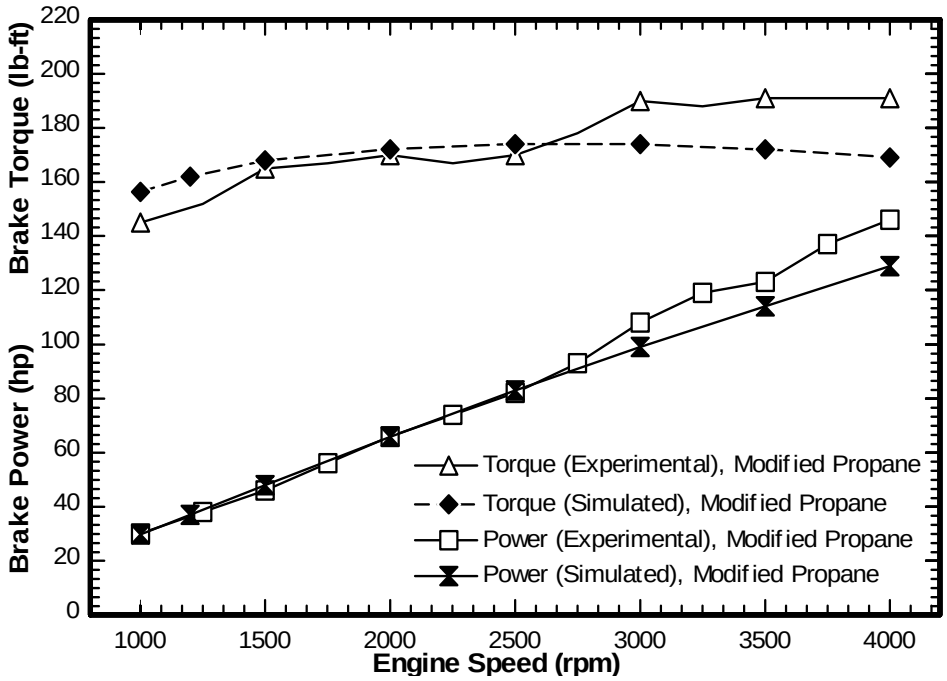

Fig. 6 Brake torque and brake horse power curves with the engine speed for 100% WOT condition for the modified propane-fuelled engine

Figure 7 shows the corresponding percentage relative difference between the brake torque and brake power values for the modified propane engine.

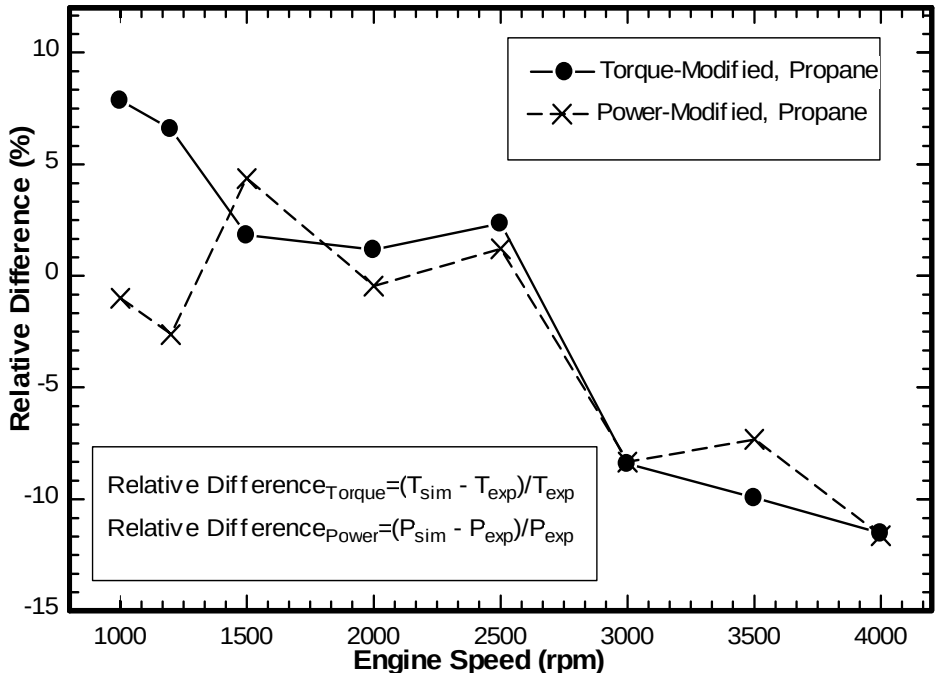

Fig. 7 Plots of percentage relative difference for brake torque and brake power with the engine speed for the modified propane-fuelled engine.

Note that the brake torque curves obtained from the simulation for all of the above cases follow the expected trend. For the cases discussed above, the brake torque curves have a value in the range of 150 to 155 lb-ft in the low engine speed range (1000 to 1500 rpm), ascend with increase in the engine speed and gain a certain maximum at approximately 2750 rpm and then descend again as the engine speed increases. This is inline with the expected behavior because as the engine speed increases, friction becomes more prominent and as a consequence causes a drop in the engine performance parameters such as efficiency and the brake torque.

This completes the discussion of the validation of the extended thermodynamic model for propane. Experimentally determined brake torque and brake power values have been compared with the corresponding simulated values at 100% WOT conditions. The values obtained from the simulation have shown acceptable degree of correlation with the experimentally determined values. Brake torque and brake power curves obtained from the simulated values follow trends similar to the corresponding curves from experimentally determined data.

6. RESULTS AND DISCUSSION

6.1 Engine Specifications

A 3.3 liter, V 6, Chrysler Minivan engine was selected for the present study. Table 5 presents the details of the engine design used and other specifications.

Table 5 Engine specifications [**4**]

Engine Type	*V6, 60°*
Engine Displacement (lit.)	3.3 liters
Compression Ratio (original)	8.9:1
Compression Ratio (modified)	11.0:1
Bore x Stroke (mm)	93 x 81
Horsepower (hp)	158 @ 4850 rpm
Brake Torque (lb-ft)	203 @ 3250 rpm
Valve Configuration	OHV, Roller Lifter

6.2 Study Methodology

The following section illustrates the methodology for conducting the parametric study. First a set of operating conditions are selected which are representative of the typical conditions and these conditions, therefore, define the base case for the parametric study. Then a structure consisting of the variables selected for conducting the parametric study is formed.

6.2.1 Operating Conditions

Ordinary spark ignition engine operation encompasses a wide range of operating modes, e.g., idle, acceleration, deceleration, and cruise. Previous analyses [**15**] suggest

that the results of a parametric study are most useful if the engine speed and load are held constant at some selected values which are representative of the typical operating modes. Therefore, for the present study, a moderate vehicle acceleration point for an engine speed of 1400 rpm and a load of approximately 325 kP, which generates a corresponding brake torque of 149 N-m, was chosen as the primary reference point. Additional computations were done at 700 rpm and 2800 rpm. The corresponding bmeps for these engine speed conditions were 164 kPa and 656 kPa respectively, resulting in corresponding brake torques of 75 N-m and 298 N-m.

In addition to the load and speed, the engine variables selected for the parametric analysis were: equivalence ratio (Φ), burn duration ($\Delta\theta_b$), combustion timing relative to MBT (θ_o), percentage exhaust gas recycle (%EGR), and compression ratio. Table 6 lists the organization of the parametric study; in each part of the study all variables were held constant at a base value except for two which were varied over the range shown.

The combustion duration ($\Delta\theta_b$) was treated as an adjustable parameter. Series of computations were made with the combustion duration held constant, while the other parameters were varied. Combustion timing was related to the timing which gave the maximum brake torque. MBT start of combustion timing was determined from the plots of $imep_{net}$ vs θ_0 and was found to be essentially independent of equivalence ratio and percentage EGR for a given engine geometry, engine speed and combustion duration. To maintain $imep_{net}$ (= bmep+fmep) constant at the chosen load-speed point as other parameters were varied, the inlet pressure (P_{in}) was varied in the simulation input.

Table 6 Structure of the parametric study

Parameters to vary	*BMEP (kPa)*	*Engine Speed (rpm)*	*ER (Φ)*	*Spark Timing (°CA relative to MBT)*	*Burn Duration (°CA)*	*EGR (%)*	r_c
Load/Speed	165-655	700-2800	1.0	MBT	60	0	11.7
Timing/Burn Duration	325	1400	1.0	-20 to +5	20-100	0	11.7
Φ /Burn Duration	325	1400	0.6-1.2	MBT	20-100	0	11.7
EGR/Burn Duration	325	1400	1.0	MBT	20-100	0-20	11.7
EGR/Timing	325	1400	1.0	-20 to +5	60	0-20	11.7
CR/Burn Duration	325	1400	1.0	MBT	40-100	0	6-13

6.3 Base Operating Conditions

The base operating point for the parametric study was chosen to be at an engine speed of 1400 rpm, load as 325 kPa, Φ = 1.0, 0% EGR, MBT timing, 60° burn duration, and 11.7:1 as the compression ratio. At this load and speed, the computed value of fmep was 75 kPa, while the $imep_{net}$ was approximately 400 kPa. The input data for this base case calculation is presented in Table 7. Cylinder volume, inlet and exhaust mass flow rates, cylinder pressure, mass fraction burned, unburned and burned gas temperatures,

nitric oxide concentration, and heat transfer rates are some of the parameters which the simulation computes as a function of crank angle.

Table 7 Input for the simulation for the base operating conditions

Engine Design and Operating Variables	*Base Condition Value for the Iso-octane-fuelled Engine*	*Base Condition Value for the Propane-fuelled Engine*
Equivalence Ratio (Φ)	1.0	1.0
Exhaust Gas Recycle Fraction (%)	0	0
Start of combustion timing (θ_o)	- 18° BTDC	- 19° BTDC
Combustion Duration ($\Delta\theta_b$)	60°	60°
Engine Speed (rpm)	1400	1400
Calorific Value (kJ/kg)	44,400	46,800
Inlet Manifold Pressure (kPa)	47.3	46.2

Table 8 presents some of the engine performance parameters generated by the simulation as part of the output. The results are presented for both the propane-fuelled and the iso-octane-fuelled engine for the base case operating conditions. Load is maintained constant at 325 kPa for the base operating conditions.

Table 8 Output from the simulation for the base operating conditions

Performance Parameter	*Simulated values for the iso-octane fuelled engine*	*Simulated values for the propane fuelled engine*
Brake Mean Effective Pressure (bmep, kPa)	325	325
Brake Specific Fuel Consumption (bsfc, g/kw-hr)	292.4	282.6
Brake Thermal Efficiency (%)	27.73	27.48
Brake Specific NO_x Emissions (bsNO, gNO/kw-hr)	5.31	5.24
Mean Exhaust Temperature (T_{exh}, K)	1006	986

As documented previously, MBT spark timing was determined from the plots of $imep_{net}$ vs θ_o. Figure 8 shows a typical plot for the base case combustion duration of $\Delta\theta_b=60°$ for the iso-octane-fuelled engine. This approach was followed throughout to determine the optimum spark timing for both propane-fuelled and the iso-octane-fuelled engine.

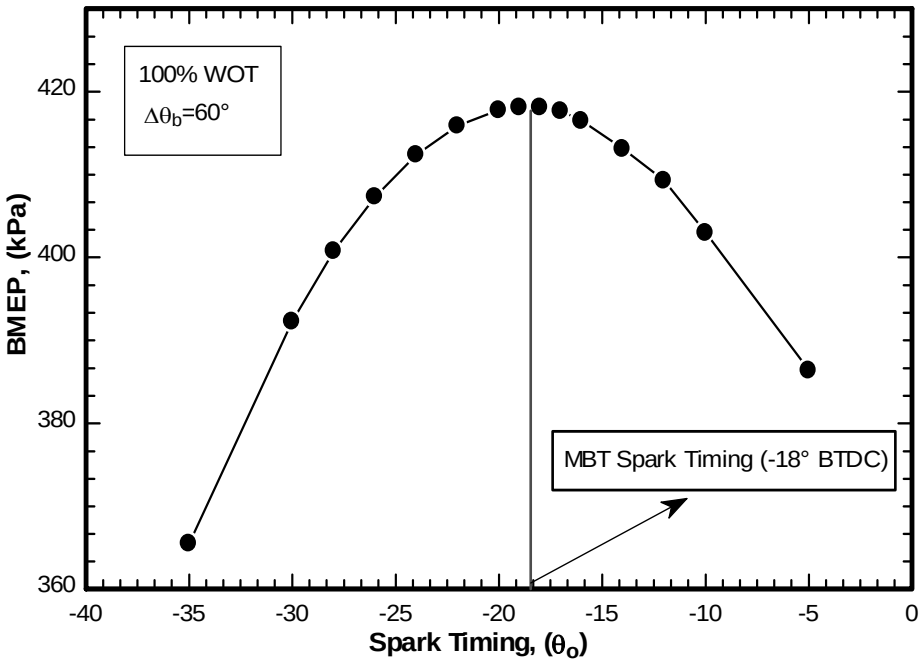

Fig. 8 Plot of bmep with spark timing to determine the optimum timing for the best torque

6.4 Results of the Parametric Study

Results of the parametric study are presented for both propane-fuelled and the iso-octane-fuelled engine. The parameters listed in Table 6 previously are considered sequentially for the analysis. The results are presented using both the absolute values from the simulation as well as the percentage relative difference for the performance parameters between the propane-fuelled and the iso-octane-fuelled engine. As documented previously, the percentage relative difference for bsfc, bsNO, and T_{exh} is defined as,

$$\text{Percentage Relative Difference (bsfc)} = \frac{\text{BSFC}_{\text{propane}} - \text{BSFC}_{\text{iso-octane}}}{\text{BSFC}_{\text{iso-octane}}} \times 100 \qquad (21)$$

$$\text{Percentage Relative Difference (bsNO)} = \frac{\text{BSNO}_{\text{propane}} - \text{BSNO}_{\text{iso-octane}}}{\text{BSNO}_{\text{iso-octane}}} \times 100 \qquad (22)$$

$$\text{Percentage Relative Difference}\,(T_{exh}) = \frac{\text{Texh}_{\text{propane}} - \text{Texh}_{\text{iso-octane}}}{\text{Texh}_{\text{iso-octane}}} \times 100 \qquad (23)$$

6.4.1 Equivalence Ratio and Combustion Duration Variation

The effects of variations in the equivalence ratio on bsfc at three different combustion durations of 20°, 60°, and 100° for both propane-fuelled and iso-octane-fuelled engine are shown in Figure 9. The simulation predicts a sharp corner in the bsfc and exhaust temperature curves at the stoichiometric point Φ =1.0 [**15**].

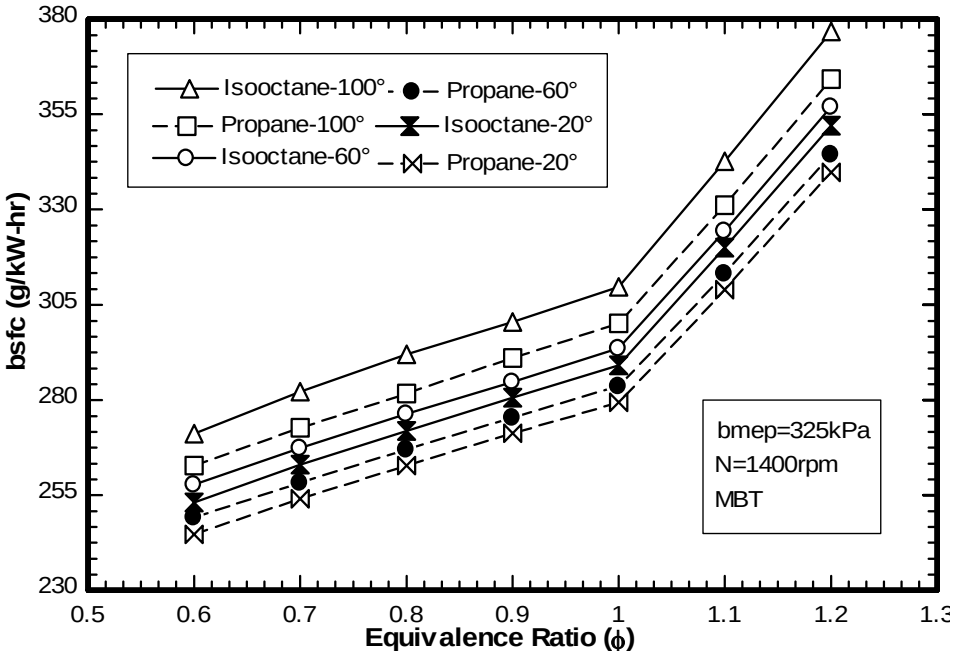

Fig. 9 Variation in brake specific fuel consumption (bsfc) with equivalence ratio at combustion durations of 20°, 60°, and 100° for both propane-fuelled and the iso-octane-fuelled engine

It can be noted from Figure 9, that the bsfc values consistently increase as the combustion duration increases from 20° to 100° for both propane-fuelled and the iso-octane-fuelled engine. At constant combustion duration, bsfc increases linearly in the

rich and lean operating range with increasing Φ for both propane-fuelled and the iso-octane-fuelled engine. For mixtures lean of stoichiometric, the theoretical fuel conversion efficiency increases linearly for $\Phi < 1.0$ as efficiency is inversely proportional to the bsfc for a particular fuel. This observation may be attributed to the fact that the combustion of mixtures leaner than stoichiometric produces products at lower temperatures, and therefore causes less dissociation of the tri-atomic molecules CO_2 and H_2O. As a consequence, the fraction of the chemical energy of the fuel which is released as sensible energy near TDC is greater; hence a greater fraction of the fuel's energy is transferred as work to the piston during the expansion stroke and the fraction of the fuel's available energy rejected to the exhaust system decreases.

For a clear understanding of the plots from Figure 9, individual plots for each combustion duration are presented separately for both propane fuelled and the iso-octane fuelled engine. Figure 10 shows the individual variation in bsfc with equivalence ratio, separately for 20° combustion duration.

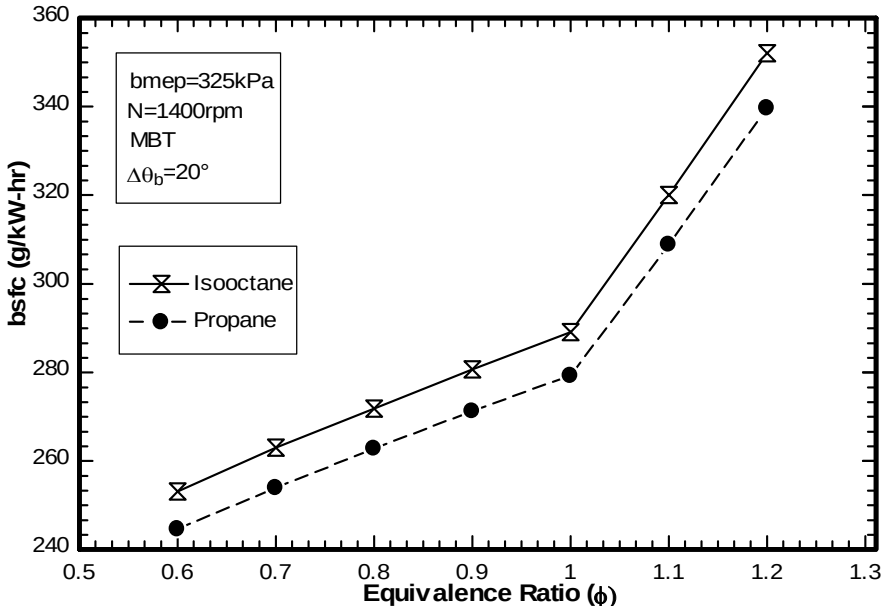

Fig. 10 Variation in brake specific fuel consumption (bsfc) with equivalence ratio at 20° combustion duration for both propane-fuelled and the iso-octane-fuelled engine

Figure 11 shows the variation in bsfc with equivalence ratio separately for 60° combustion duration. It is noted that the values of bsfc for propane-fuelled engine are consistently lower than the corresponding values for the iso-octane-fuelled engine for all combustion durations. This difference in the bsfc values can be attributed to the dissimilar heating values of the two fuels. On a mass basis, the calorific value of propane (46,800 kJ/kg) is higher than that of iso-octane (44,400 kJ/kg). Consequently for the same mass of the two fuels, the power ouput from the engine fuelled by propane would be higher than that generated by the iso-octane-fuelled engine. Therefore, the values of bsfc generated by the propane fuelled engine would be lower than the corresponding values from the iso-octane fuelled engine.

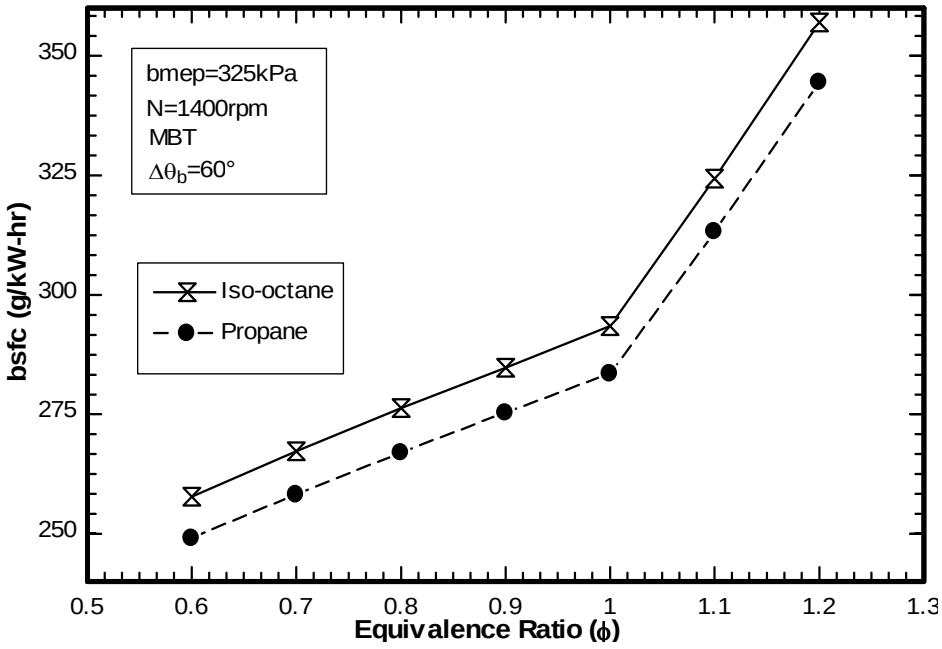

Fig. 11 Variation in brake specific fuel consumption (bsfc) with equivalence ratio at 60° combustion duration for both propane-fuelled and the iso-octane-fuelled engine

Figure 12 shows the variation in bsfc with equivalence ratio separately for the combustion duration of 100°. It is observed that the bsfc values from the propane-fuelled engine are consistently lower than the corresponding values from the iso-octane-fuelled engine for the combustion duration of 100°. While low values of bsfc are always desirable, it cannot be readily concluded from these results that propane would result in higher thermal efficiency, as the heating values of the two fuels under consideration are different. It is noted that the relative difference between the bsfc values for the two fuels under consideration is approximately the same for all combustion durations and equivalence ratios.

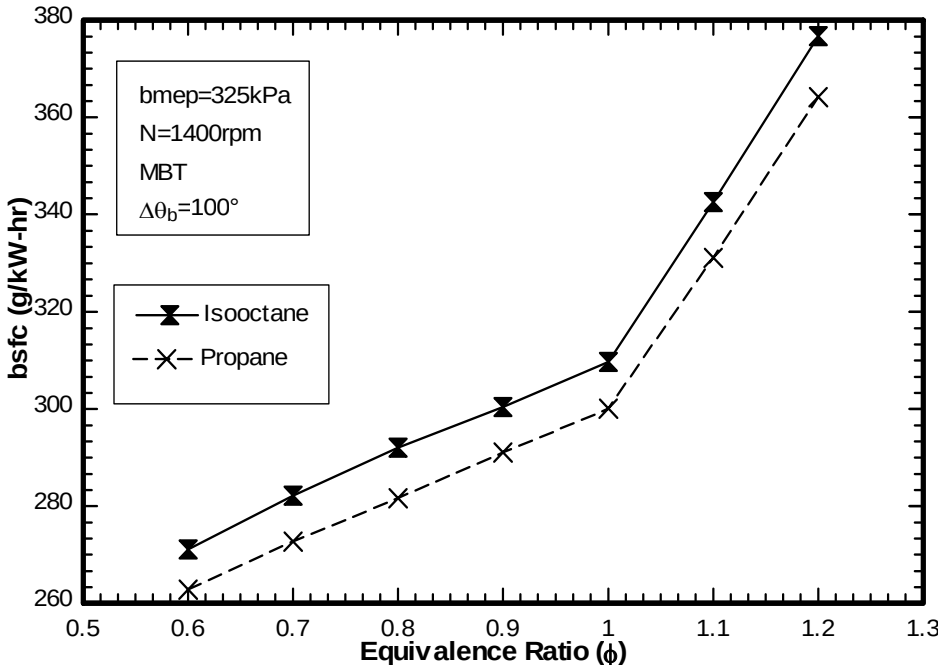

Fig. 12 Variation in brake specific fuel consumption (bsfc) with equivalence ratio at 100° combustion duration for both propane-fuelled and the iso-octane-fuelled engine

The effects of variations in equivalence ratio on bsNO at three different combustion durations of 20°, 60°, and 100° for both propane-fuelled and the iso-octane-fuelled engine are shown in Figure 13. The bsNO values have peak just before the stochiometric equivalence ratio of 1.0. The shape of the curve is well known for iso-octane, but the interesting observation is that the values of bsNO for both propane-fuelled and the iso-octane-fuelled engine are approximately the same. This similarity in the bsNO plots for the two fuels can be explained through their similar peak combustion temperature magnitudes.

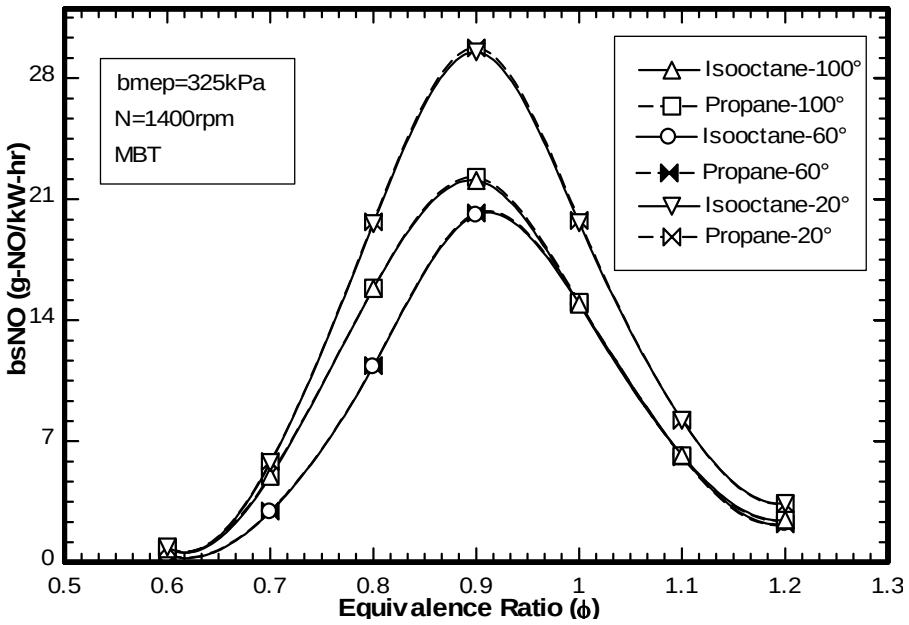

Fig. 13 Variation in brake specific nitric oxide emissions (bsNO) with equivalence ratio at combustion durations of 20°, 60°, and 100° for both propane-fuelled and the iso-octane-fuelled engine

As documented previously in the literature review, to maintain a sustained flame propagation at elevated pressures, the combustion temperatures should be approximately 1900 K or greater. If the mixture temperatures at the beginning and the end of

combustion are equal or greater than 1900 K, it is reasonable to assume that during the remainder of the combustion cycle, temperatures will be greater than 1900 K for typical operating conditions. If the mixture temperature is less than 1900 K, the mixture will not ignite for typical engine operating conditions. However, at or above such temperatures, the rate of NO_x formation is significant, regardless of the fuel's chemical composition.

In the present simulation, it is observed that the peak combustion temperatures are well in excess of 2000 K for both iso-octane and propane. Also, the peak combustion temperatures are of similar magnitude for all the simulation runs. The formation of bsNO is primarily a function of peak combustion temperature and since these temperatures are approximately the same for both propane-fuelled and the iso-octane-fuelled engine, so is the amount of bsNO formed. As a result the plots of bsNO for both propane- fuelled and the iso-octane-fuelled engine overlap.

The effects of variations in equivalence ratio on T_{exh} at three different combustion durations of 20°, 60°, and 100° for both propane-fuelled and the iso-octane fuelled engine are shown in Figure 14. The exhaust temperatures consistently increase for both propane-fuelled and the iso-octane-fuelled engine as the combustion duration increases. This is inline with the expected behavior because as the combustion duration increases, the products from combustion get lesser time to loose energy to the surroundings and as a consequence more heat is rejected through the exhaust resulting in higher temperatures.

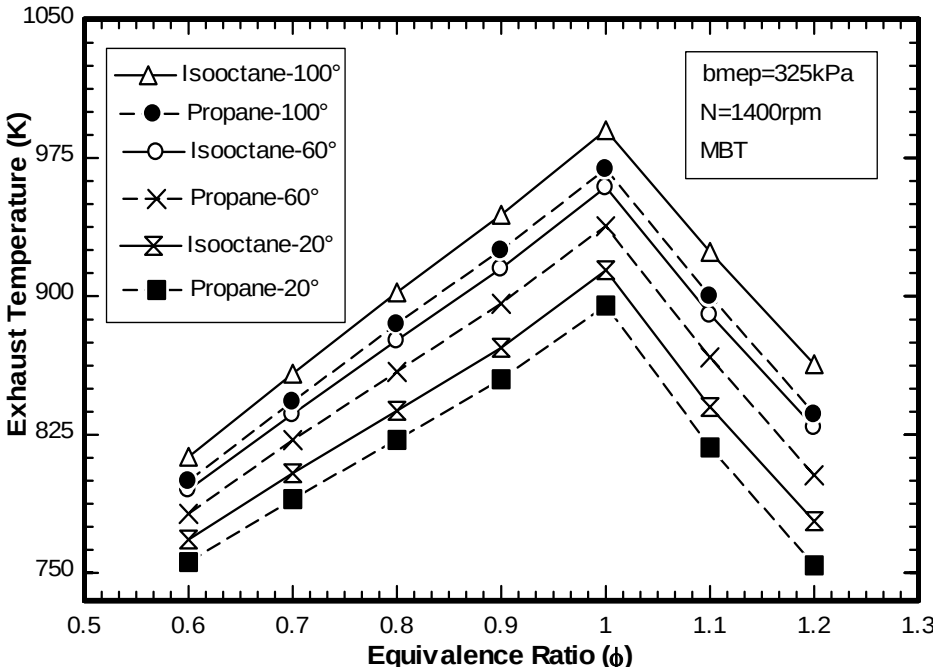

Fig. 14 Variation in mean exhaust temperature (T_{exh}) with equivalence ratio at combustion durations of 20°, 60°, and 100° for both propane-fuelled and the iso-octane-fuelled engine

For a clear understanding of the plots from Figure 14, individual plots for each combustion duration are presented separately for both propane-fuelled and the iso-octane- fuelled engine. Figure 15 shows the individual variation in T_{exh} with equivalence ratio, separately for 20° combustion duration.

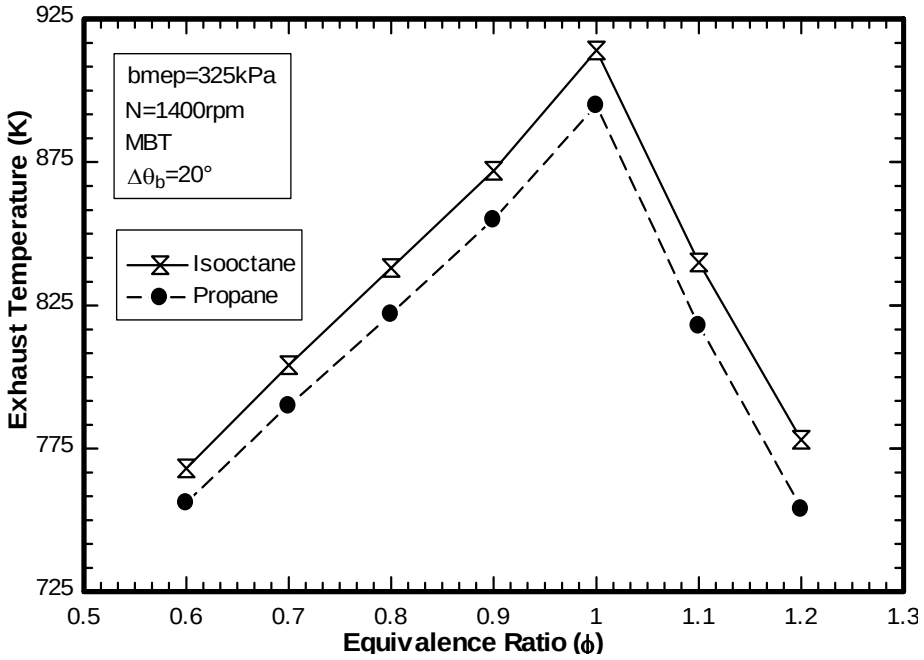

Fig. 15 Variation in mean exhaust temperature (T_{exh}) with equivalence ratio at 20° combustion duration for both propane-fuelled and the iso-octane-fuelled engine

The lower values of the mean exhaust temperatures for propane relative to iso-octane is a consequence of the different exhaust mixture compositions. The chemical formula of iso-octane is C_8H_{18}, while that of propane is C_3H_8. The mole fraction of H_2O in the exhaust mixture for the iso-octane fuelled engine is lesser than that in the exhaust mixture for the propane-fuelled engine. Also, the mole fraction of CO_2 in the exhaust mixture for the iso-octane-fuelled engine is greater than that for the propane-fuelled engine. Since the specific heat of H_2O is lower than that of CO_2, the exhaust gas mixture for the propane fuelled engine is cooled to a greater extent for the same heat loss.

Figure 16 shows the same variation in the T_{exh} with equivalence ratio separately for the combustion duration of 60°. It is observed that the mean exhaust temperatures for the iso-octane-fuelled engine were consistently higher than the corresponding temperatures for the propane-fuelled engine for all combustion durations.

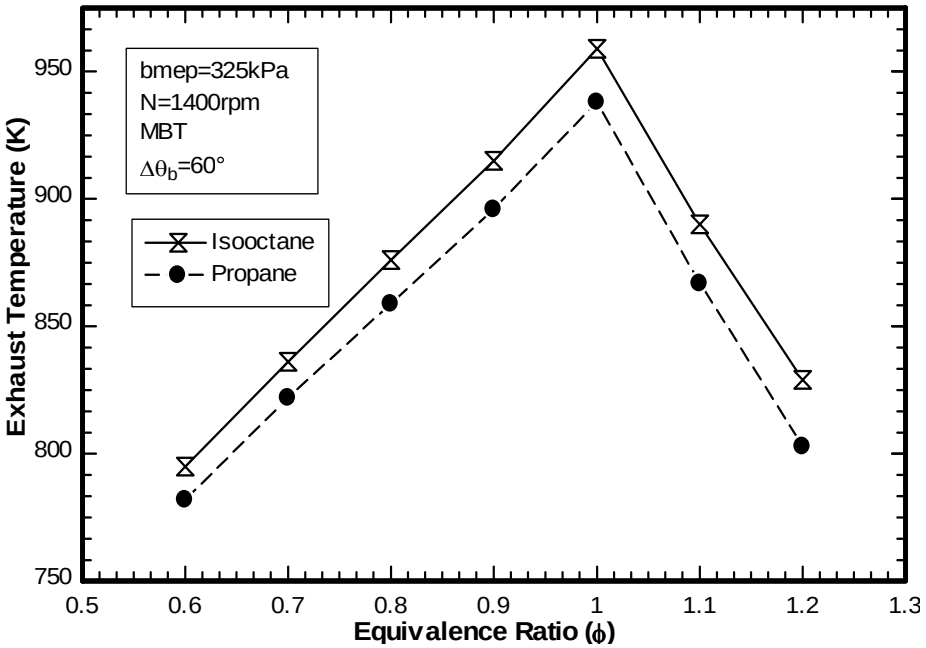

Fig. 16 Variation in mean exhaust temperature (T_{exh}) with equivalence ratio at 60° combustion duration for both propane-fuelled and the iso-octane-fuelled engine

Figure 17 shows the same variation in the T_{exh} with equivalence ratio separately for the combustion duration of 100°. It is observed that as the combustion duration increases from 20° to 100°, the magnitudes of the mean exhaust temperatures also increase correspondingly. The relative difference in the mean exhaust temperatures for both propane-fuelled and the iso-octane fuelled engine, however, remains approximately the same for all combustion durations.

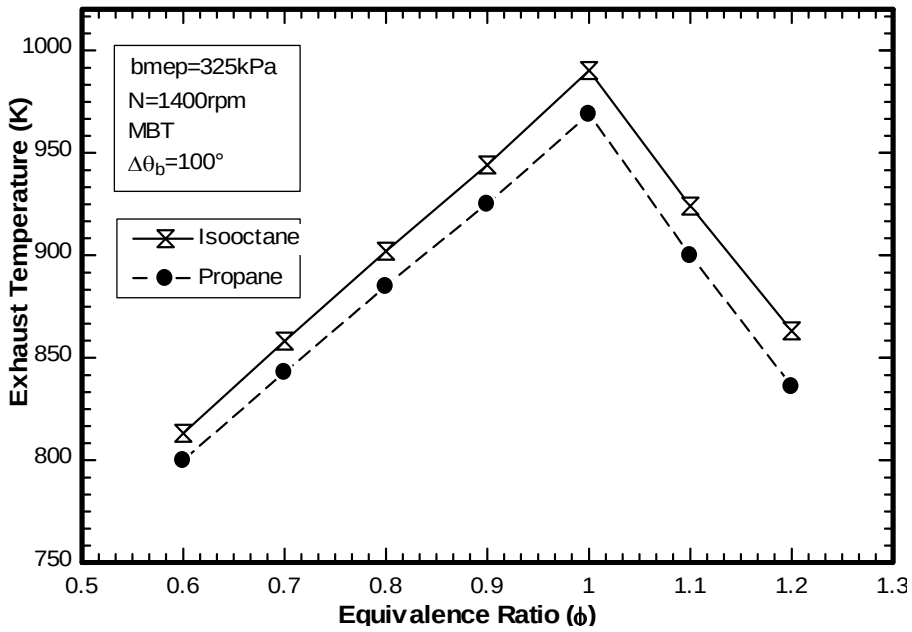

Fig. 17 Variation in mean exhaust temperature (T_{exh}) with equivalence ratio at 100° combustion duration for both propane-fuelled and the iso-octane-fuelled engine

Figure 18 shows the percentage relative difference between the simulated and the experimentally determined values for bsfc, bsNO, and T_{exh} with variation in equivalence ratio for the base case combustion duration of 60°.

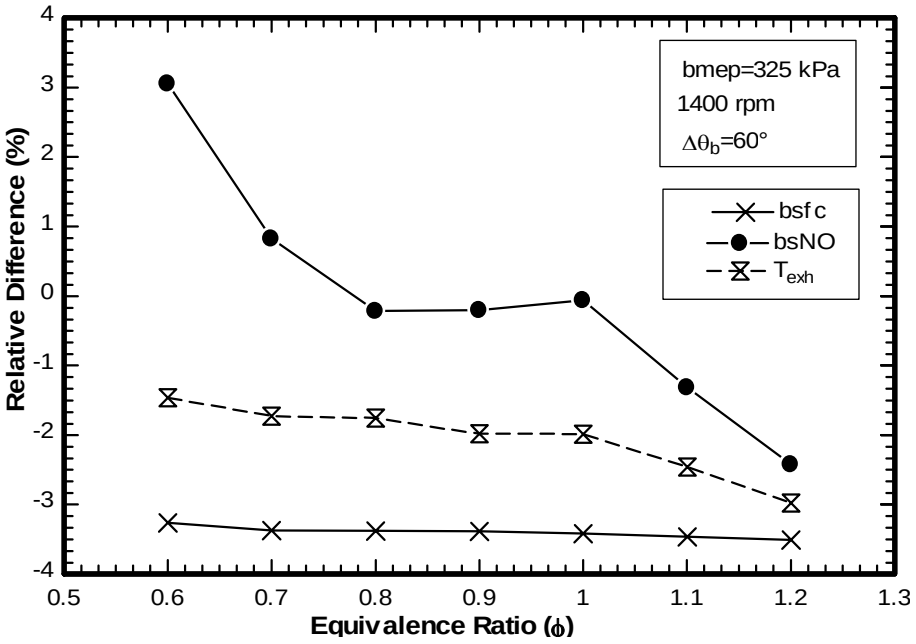

Fig. 18 Percentage relative difference between simulated and the experimental values for bsfc, bsNO, and T_{exh} with variation in equivalence ratio for the base case conditions

6.4.2 Percentage EGR and Combustion Duration Variation

The effects of variations in percentage exhaust gas recycle (%EGR) on bsfc at three different combustion durations of 20°, 60°, and 100° for both propane-fuelled and the iso-octane-fuelled engine are shown in Figure 19.

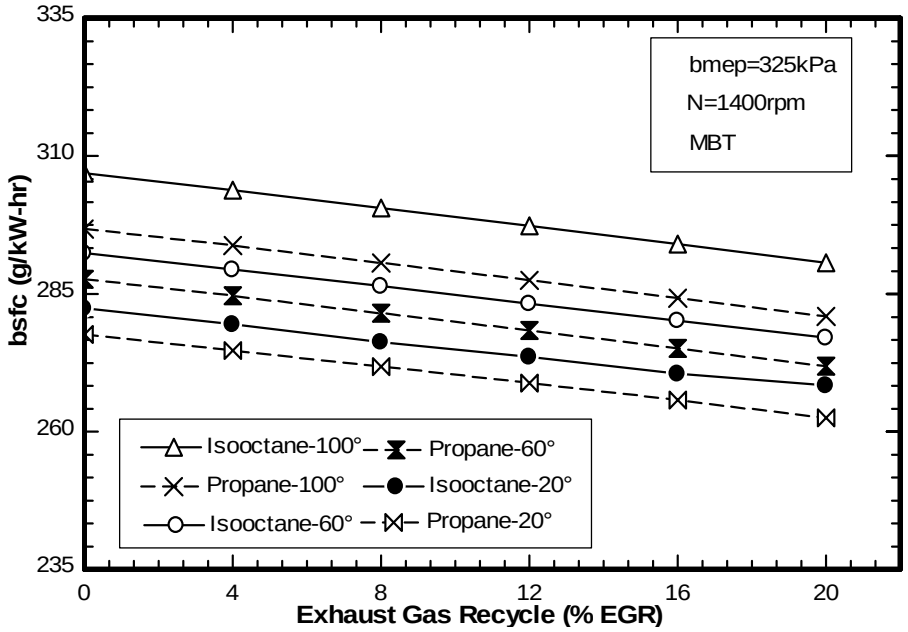

Fig. 19 Variation in brake specific fuel consumption (bsfc) with percent exhaust gas recycle at combustion durations of 20°, 60°, and 100° for both propane-fuelled and the iso-octane-fuelled engine

Percentage EGR has a more pronounced effect on bsfc, bsNO, and T_{exh} than the combustion duration. For the operating conditions of this study, bsfc and exhaust temperature decrease with increasing EGR for both fuels under consideration. The dilution improves efficiency by decreasing pumping work and by making the thermodynamic properties more favorable (cp/cv increases with increasing EGR) [**15**]. Also, there is reduced heat loss to the walls because the combustion temperatures decrease considerably. As a consequence, there is a reduction in the degree of

dissociation in the high-temperature burned gases, which allows more of the fuel's chemical energy to be converted to sensible energy near TDC.

For a clear understanding of the plots from Figure 19, individual plots for each combustion duration are presented separately for both propane-fuelled and the iso-octane-fuelled engine. Figure 20 shows the individual variation in bsfc with %EGR separately for combustion duration of 20°.

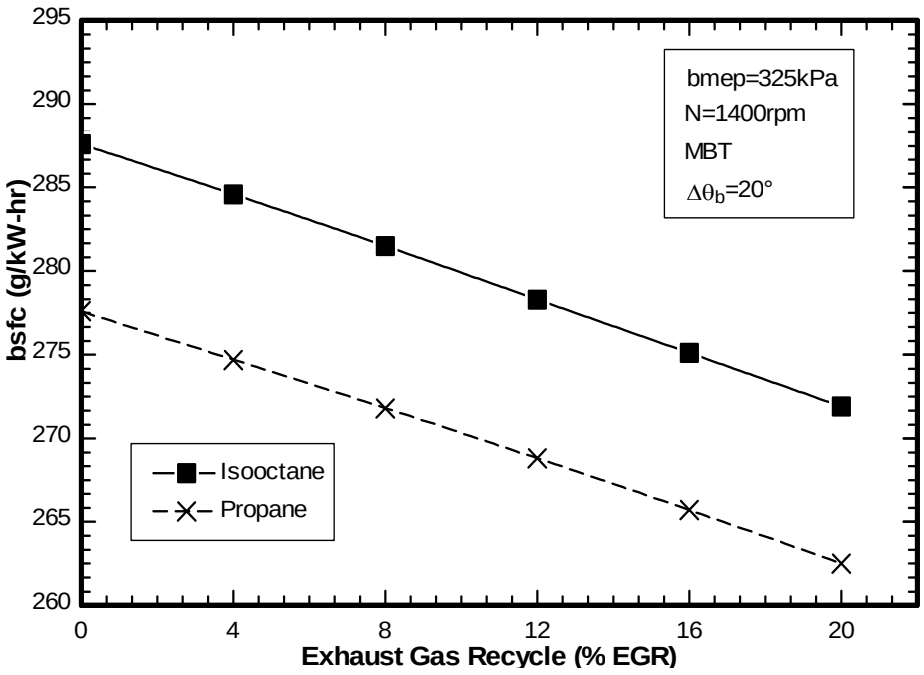

Fig. 20 Variation in brake specific fuel consumption (bsfc) with percent exhaust gas recycle at 20° combustion duration for both propane-fuelled and the iso-octane-fuelled engine

Figure 21 shows the individual variation in bsfc with %EGR separately for 60° combustion duration as the base case for both propane-fuelled and the iso-octane-fuelled engine. The values of bsfc for propane are consistently lower than those for iso-octane for all combustion durations. As documented earlier, this difference can be attributed to the fact that the calorific value of propane (on a mass basis) is higher than the corresponding value of iso-octane.

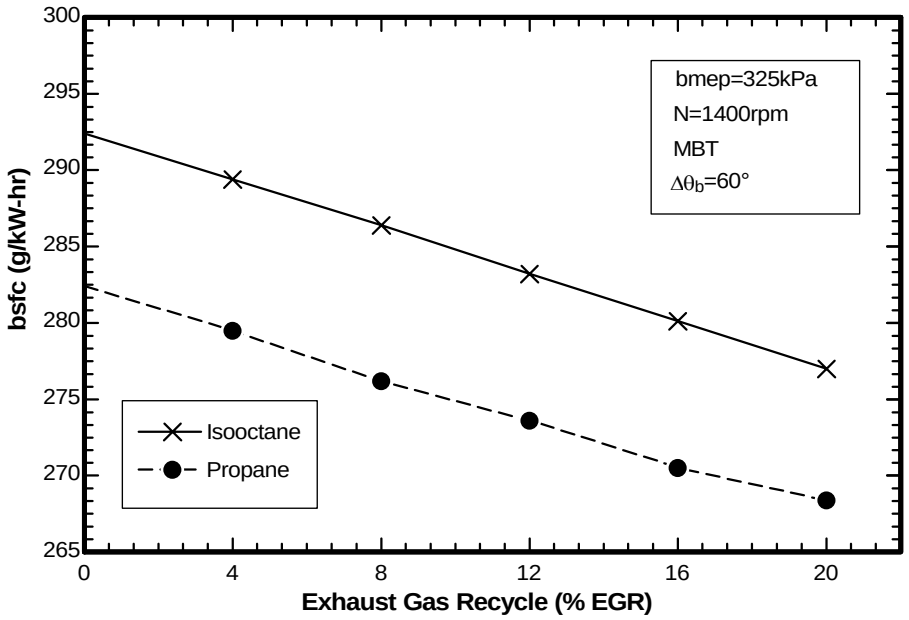

Fig. 21 Variation in brake specific fuel consumption (bsfc) with percent exhaust gas recycle at 60° combustion duration for both propane-fuelled and the iso-octane-fuelled engine

Figure 22 shows the individual variation in bsfc with %EGR separately for 100° combustion duration for both propane-fuelled and the iso-octane-fuelled engine. The relative difference in the bsfc values between propane-fuelled and the iso-octane-fuelled engine for combustion duration of 100° is marginally greater than the corresponding difference for the combustion durations of 20° and 60° respectively.

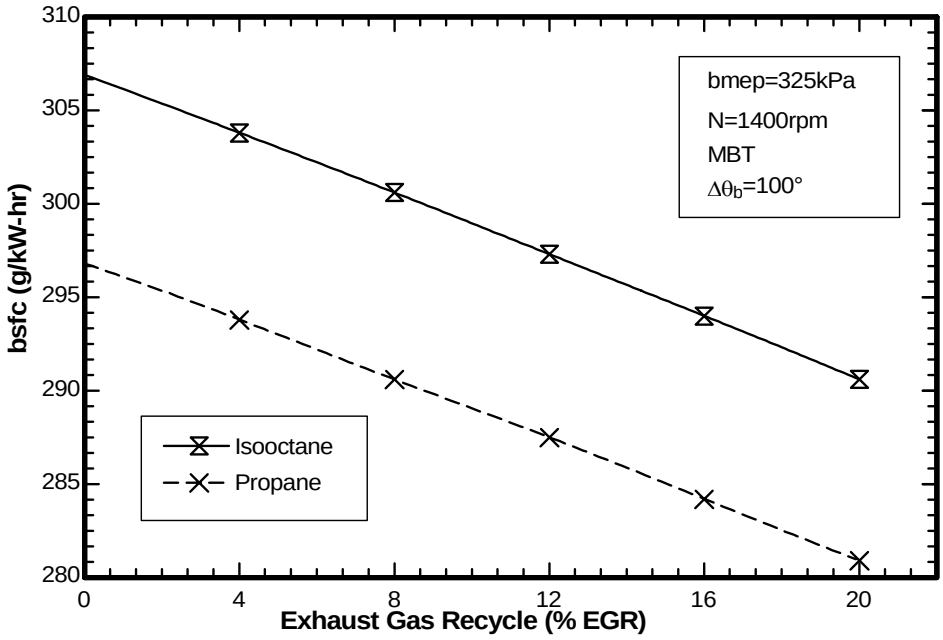

Fig. 22 Variation in brake specific fuel consumption (bsfc) with percent exhaust gas recycle at 100° combustion duration for both propane-fuelled and the iso-octane-fuelled engine

The effects of variations in percent exhaust gas recycle (%EGR) on bsNO at three different combustion durations of 20°, 60°, and 100° for both propane-fuelled and the iso-octane-fuelled engine are shown in Figure 23. As documented earlier, formation of bsNO is a function of peak combustion temperature. In the present study the peak combustion temperatures are approximately the same for both iso-octane fuelled engine and the propane fuelled engine for all %EGR values and therefore the rates of bsNO formation are of similar magnitudes.

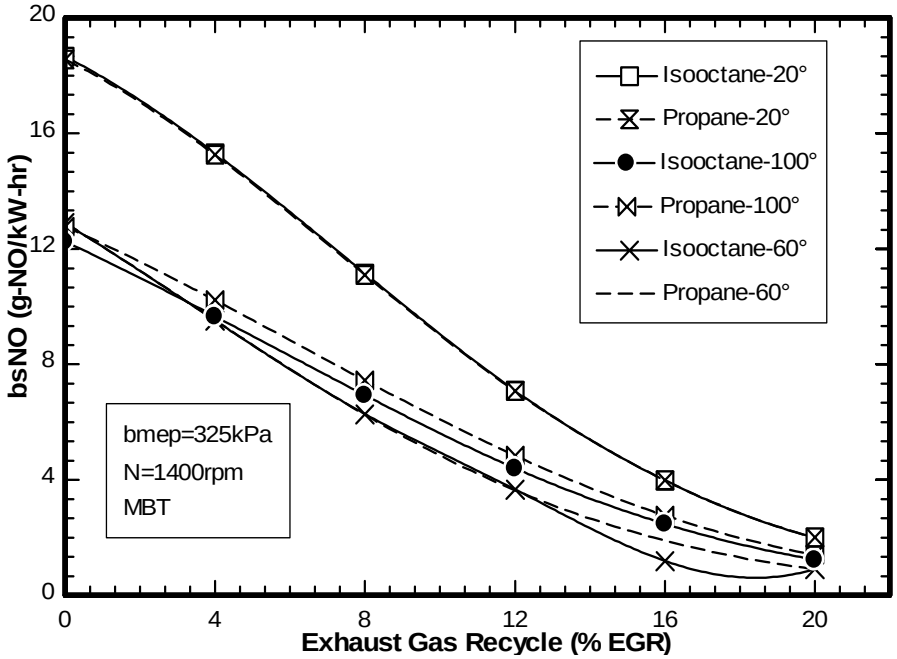

Fig. 23 Variation in brake specific nitric oxide emissions (bsNO) with percent exhaust gas recycle at combustion durations of 20°, 60°, and 100° for both propane-fuelled and the iso-octane-fuelled engine

The effects of variations in percent exhaust gas recycle (%EGR) on T_{exh} at three different combustion durations of 20°, 60°, and 100° for both propane-fuelled and iso-octane-fuelled engine are shown in Figure 24. It was observed that the mean exhaust temperatures for the propane-fuelled engine were consistently lower than the corresponding temperatures for the isooctane-fuelled engine for all combustion durations. This difference can be attributed to the different chemical structures of the two fuels resulting in their dissimilar exhaust gas mixture compositions.

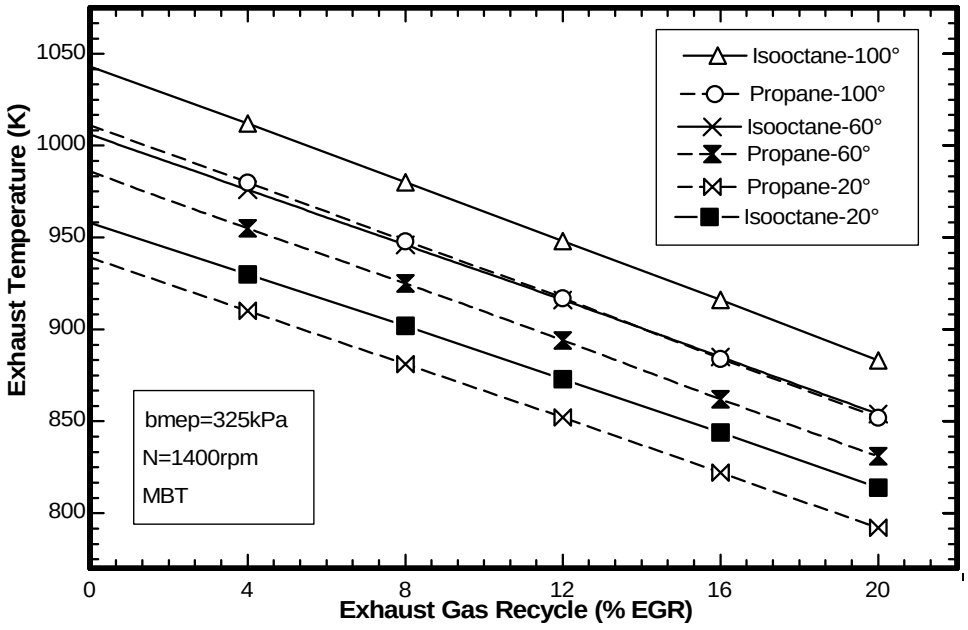

Fig. 24 Variation in mean exhaust temperature (T_{exh}) with percent exhaust gas recycle at combustion durations of 20°, 60°, and 100° for both propane-fuelled and the iso-octane-fuelled engine

For a clear understanding of the plots from Figure 24, individual plots for each combustion duration are presented separately for both propane-fuelled and the iso-octane- fuelled engine. Figure 25 shows the individual variation in T_{exh} with equivalence ratio, separately for 20° combustion duration.

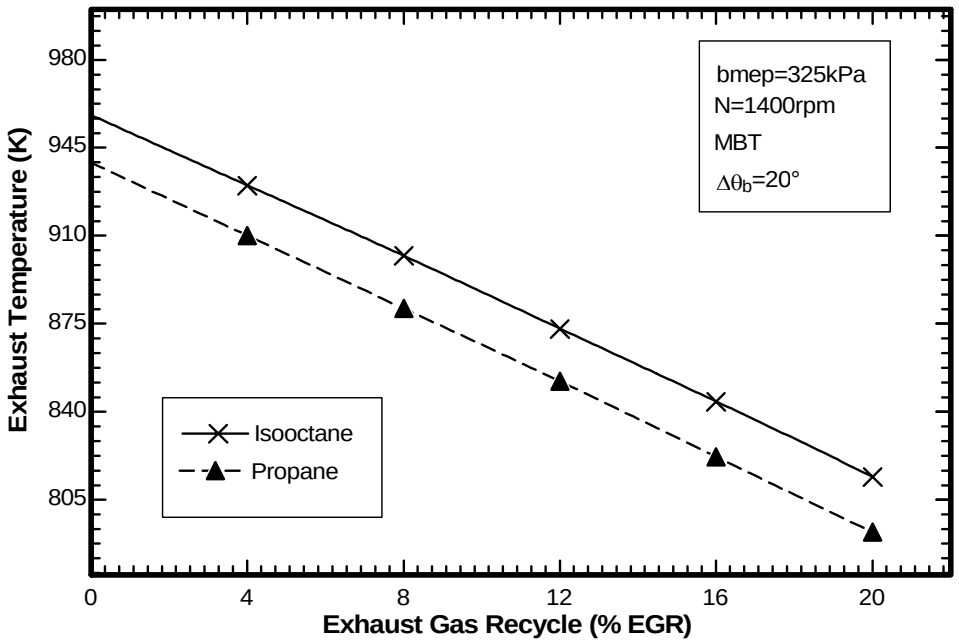

Fig. 25 Variation in mean exhaust temperature (T_{exh}) with percent exhaust gas recycle for combustion duration of 20° for both propane-fuelled and the iso-octane-fuelled engine

Figure 26 and Figure 27 show the individual variation in T_{exh} with equivalence ratio, separately for 60° and 100° combustion duration respectively.

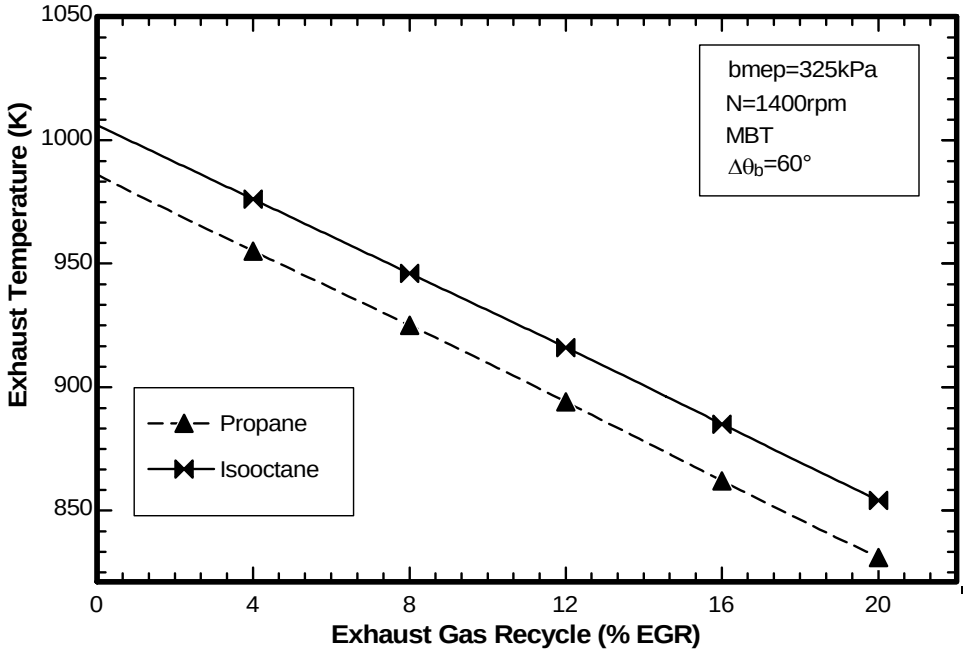

Fig. 26 Variation in mean exhaust temperature (T_{exh}) with percent exhaust gas recycle for combustion duration of 60° for both propane-fuelled and the iso-octane-fuelled engine

Figure 27 shows the same variation in the T_{exh} with equivalence ratio separately for the combustion duration as 100°. The relative difference in the T_{exh} values between the propane-fuelled and the iso-octane-fuelled engine for combustion duration as 100° is marginally greater than the corresponding difference for the combustion durations of 20° and 60° respectively.

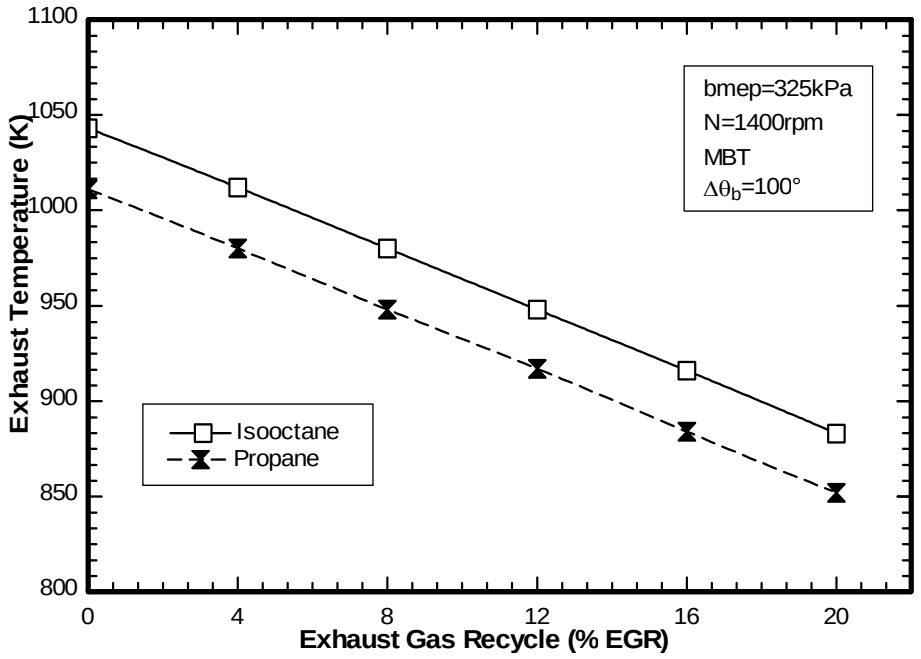

Fig. 27 Variation in mean exhaust temperature (T_{exh}) with percent exhaust gas recycle for combustion duration of 100° for both propane-fuelled and the iso-octane-fuelled engine

Figure 28 shows the percentage relative difference between the simulated and the experimentally determined values for bsfc, bsNO, and T_{exh} with variation in %EGR for the base case combustion duration of 60°.

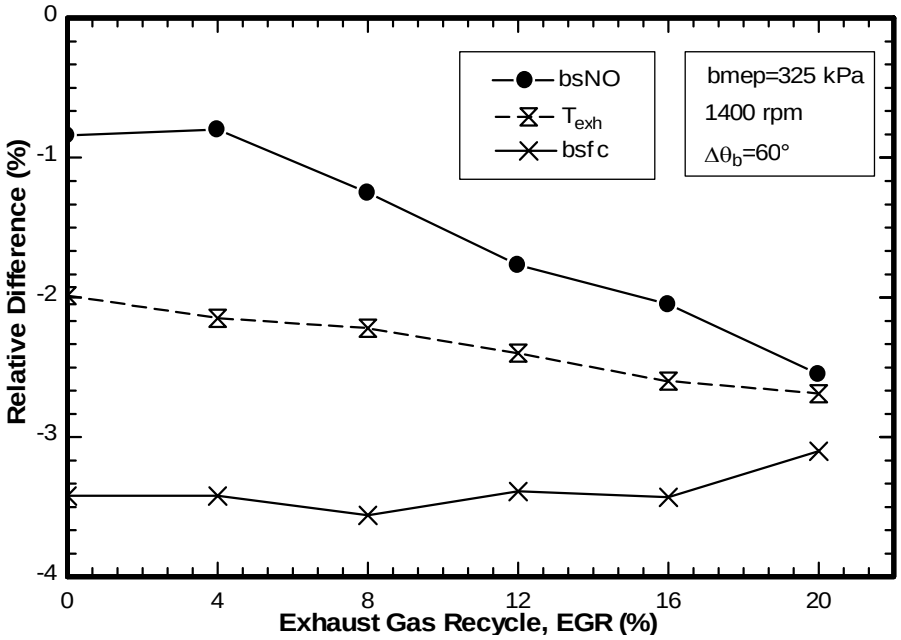

Fig. 28 Percentage relative difference between simulated and the experimental values for bsfc, bsNO, and T_{exh} with variation in %EGR for the base case conditions

6.4.3 Spark Timing and Combustion Duration Variation

The effects of changes in timing relative to the MBT on bsfc at the base operating condition for three different combustion durations of 20°, 60°, and 100° are shown for both propane-fuelled and the iso-octane fuelled engine in Figure 29. It is observed that both advanced and retarded spark timing increases bsfc for both propane-fuelled and the iso-octane-fuelled engine. This is inline with the expected behavior as MBT is determined from the plots of imep vs θ_o. On either side of the MBT, the value of imep drops. Due to the decrease in imep, the overall effect is reduced brake horse power output, leading to a reduced value of bsfc. Increasing the combustion duration increases bsfc and exhaust temperature and decreases bsNO, although to a more modest degree.

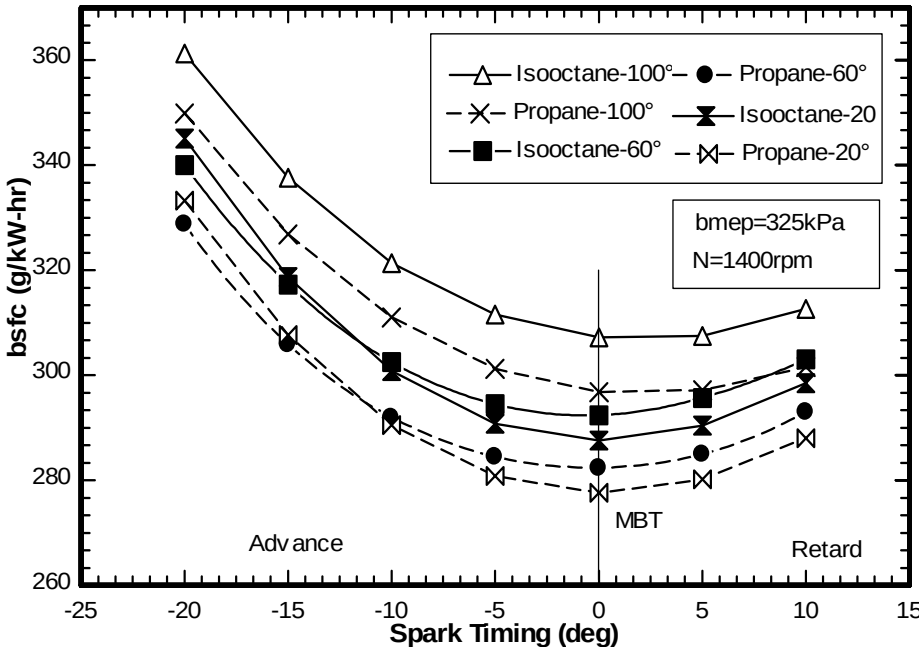

Fig. 29 Variation in brake specific fuel consumption (bsfc) with spark timing at combustion durations of 20°, 60°, and 100° for both propane-fuelled and the iso-octane-fuelled engine

For a clear understanding of the plots from Figure 29, individual plots for each combustion duration are presented separately for both propane-fuelled and the iso-octane-fuelled engine. Figure 30 shows the individual variation in bsfc with spark timing, separately for 20° combustion duration.

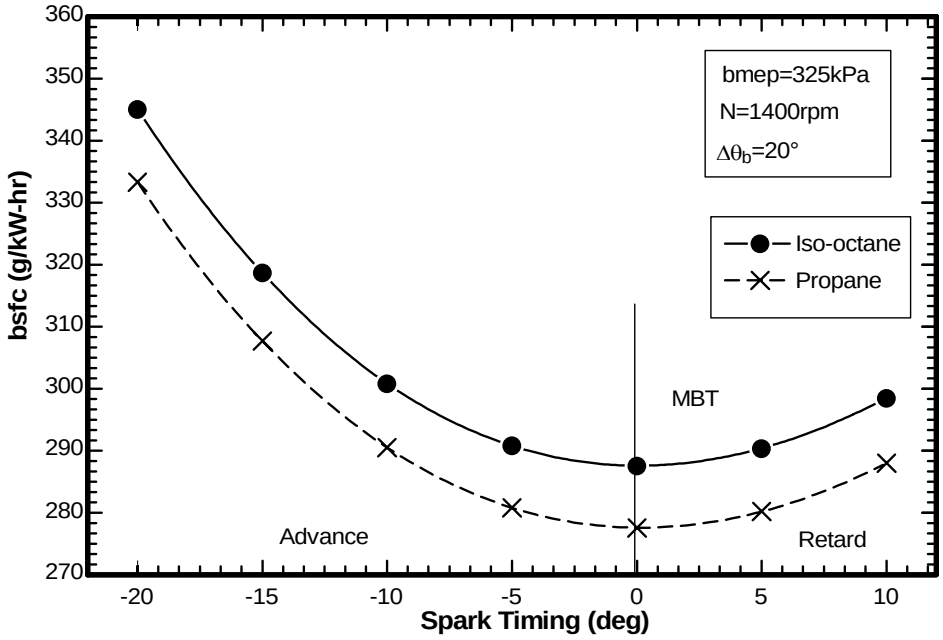

Fig. 30 Variation in brake specific fuel consumption (bsfc) with spark timing at combustion duration of 20° for both propane-fuelled and the iso-octane-fuelled engine

Figure 31 shows the individual variation in bsfc with spark timing separately for 60° combustion duration. It is observed that the bsfc values obtained for the propane-fuelled engine are consistently lower than the corresponding values for the iso-octane-fuelled engine for all combustion durations. As documented previously, this observation can be attributed to the fact that the calorific values of the two fuels under consideration are different. For the same brake power from both iso-octane-fuelled and propane-fuelled engine, propane because of its higher calorific value would require less mass compared to iso-octane during a given amount of time. This is the reason for propane-fuelled engine's consistently lower bsfc values than the corresponding values from iso-octane fuelled engine for all the combustion durations.

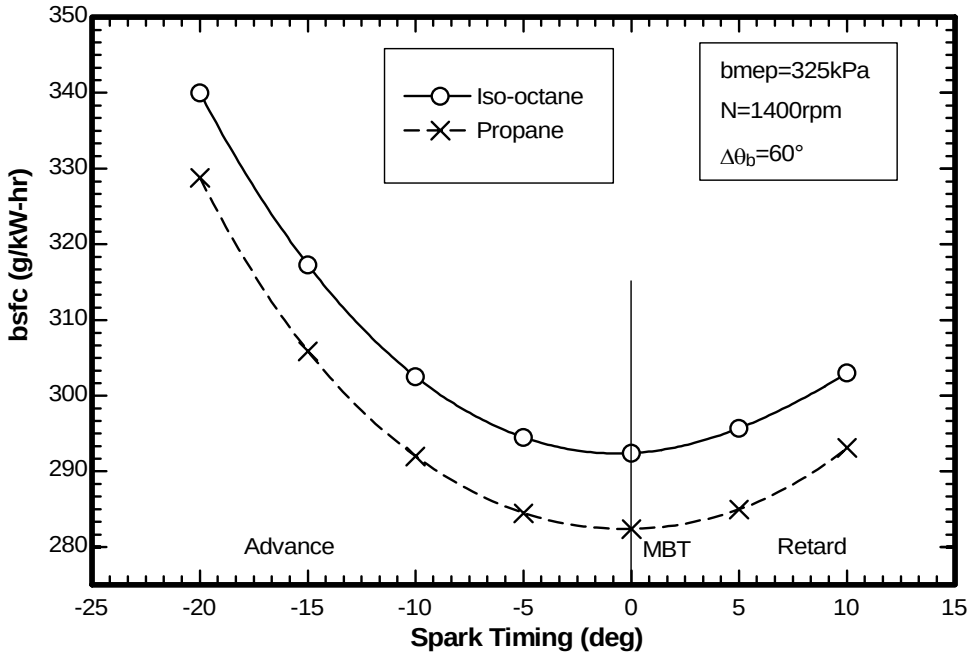

Fig. 31 Variation in brake specific fuel consumption (bsfc) with spark timing at combustion duration of 60° for both propane-fuelled and the iso-octane-fuelled engine

Figure 32 shows the individual variation in bsfc with spark timing separately for 100° combustion duration. The absolute values of bsfc consistently increase as the combustion duration increases from 20° to 100°. The percentage relative difference in the bsfc values for all the combustion durations are approximately the same for both propane-fuelled and the iso-octane fuelled engine.

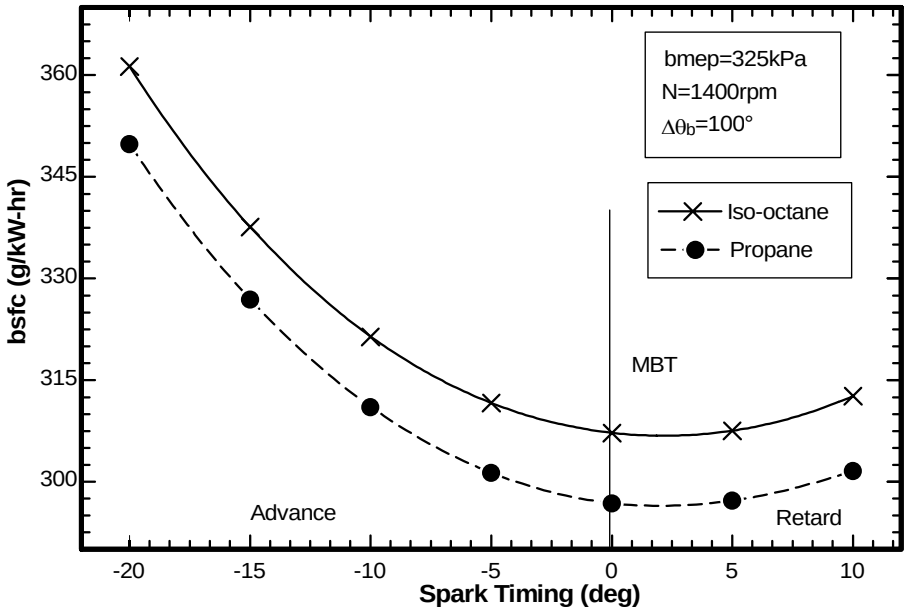

Fig. 32 Variation in brake specific fuel consumption (bsfc) with spark timing at combustion duration of 100° for both propane-fuelled and the iso-octane-fuelled engine

Figure 33 shows the effects of variation in spark timing on T_{exh} for combustion durations of 20° and 100° for both propane-fuelled and the iso-octane-fuelled engine. Retarded timing causes the combustion to occur late during the cycle and as a consequence, the products of combustion have lesser time to loose heat to the surroundings during the expansion cycle. This correspondingly increases the exhaust temperatures.

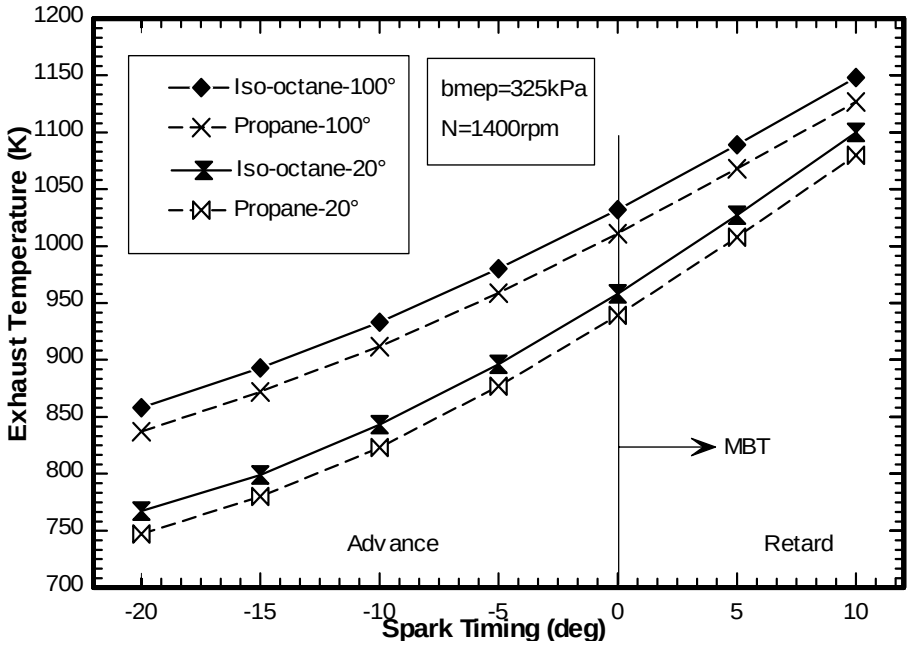

Fig. 33 Variation in mean exhaust temperature (T_{exh}) with spark timing for combustion durations of 20° and 100° for both propane-fuelled and the iso-octane-fuelled engine

Figure 34 shows the percentage relative difference between the simulated and the experimentally determined values for bsfc, bsNO, and T_{exh} with variation in the spark timing for the base case operating conditions.

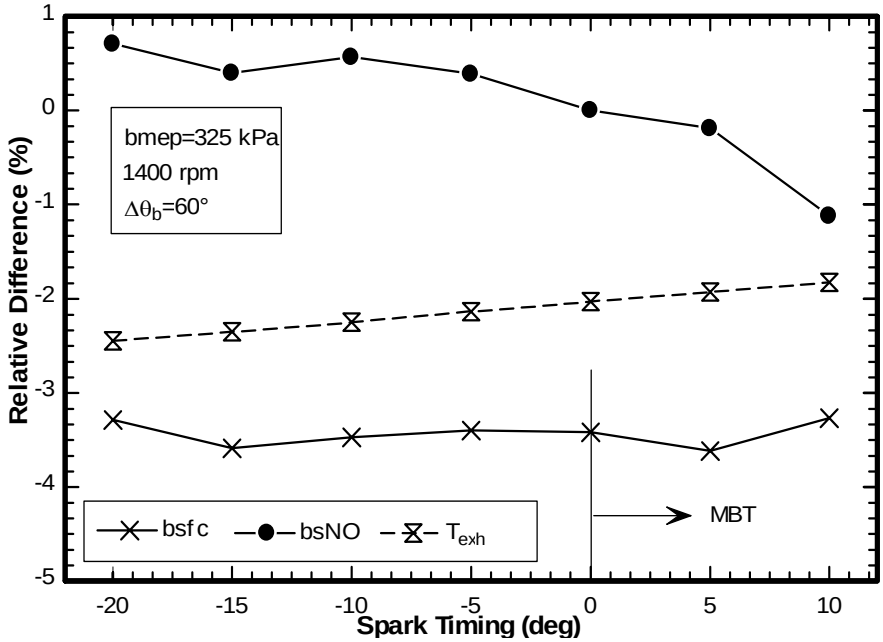

Fig. 34 Percentage relative difference between the simulated and the experimentally determined values of bsfc, bsNO, and T_{exh} with variation in spark timing for the base case conditions

6.4.4 Compression Ratio and Combustion Duration Variation

Variation in compression ratio significantly affects bsfc, theoretical fuel conversion efficiency and the exhaust temperatures. The effect on bsNO is relatively much more modest. The effects of variations in compression ratio on bsfc at three different combustion durations of 40°, 60°, and 100° for both propane-fuelled and the iso-octane-fuelled engine are shown in Figure 35.

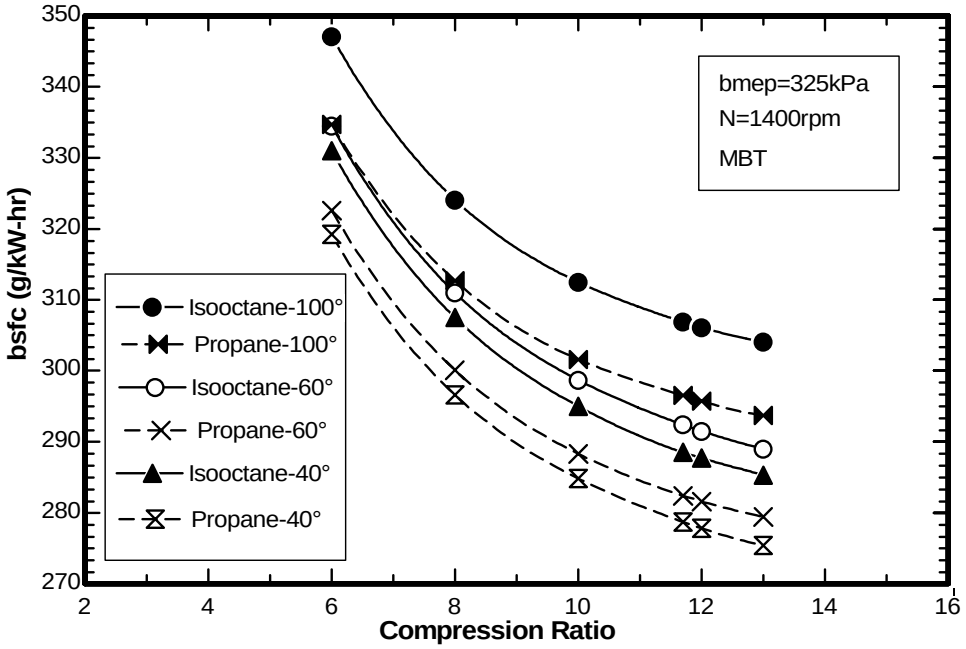

Fig. 35 Variation in brake specific fuel consumption (bsfc) with compression ratio at combustion durations of 40°, 60°, and 100° for both propane-fuelled and the iso-octane-fuelled engine

For a clear understanding of the plots from Figure 35, individual plots for each combustion duration are presented separately for both propane-fuelled and the iso-octane-fuelled engine. Figure 36 shows the individual variation in bsfc with compression ratio, separately for 40° combustion duration.

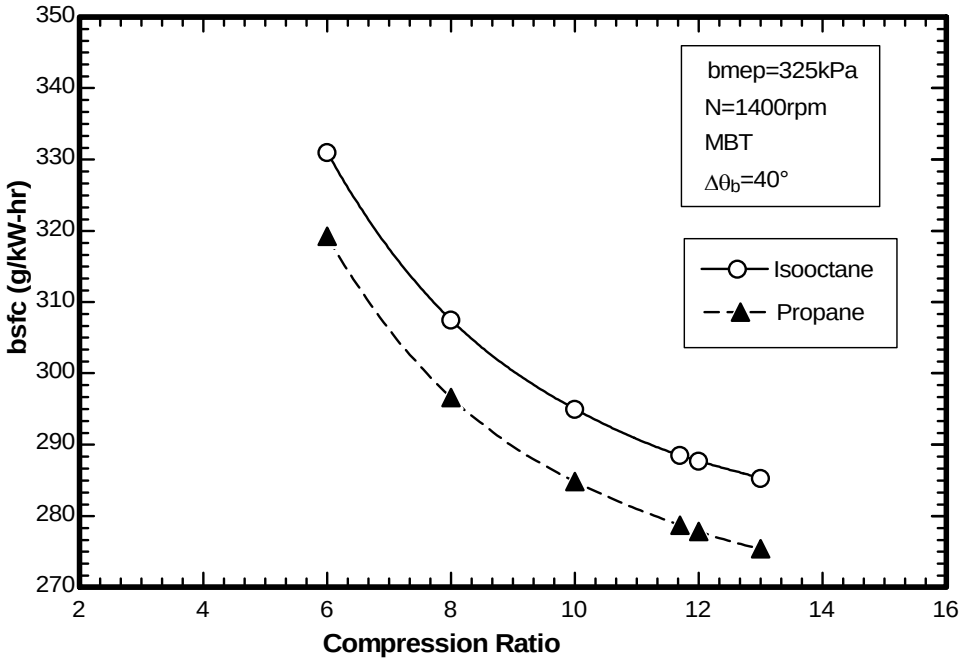

Fig. 36 Variation in brake specific fuel consumption (bsfc) with compression ratio at combustion duration of 40° for both propane-fuelled and the iso-octane-fuelled engine

Figure 37 shows the same variation separately for the base case combustion duration of 60°. Again it is noted that the bsfc values for the propane-fuelled engine are consistently lower than the corresponding values for the iso-octane-fuelled engine. As documented earlier, the calorific values of the two fuels under consideration are different. Therefore, the corresponding difference in the bsfc values obtained for the propane fuelled and the iso-octane fuelled engine can be attributed to dissimilar heating values for the same amount of fuel burned.

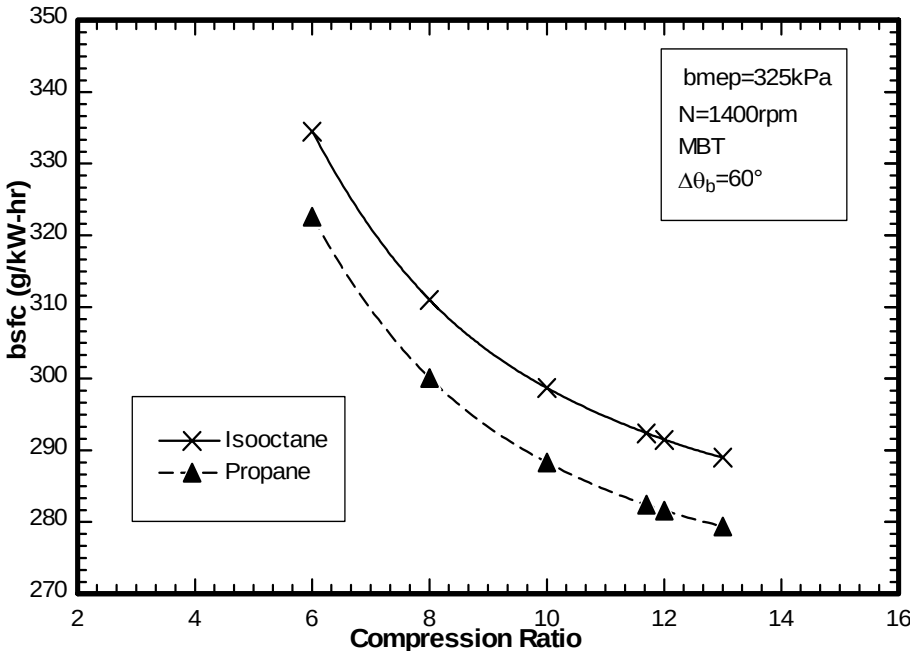

Fig. 37 Variation in brake specific fuel consumption (bsfc) with compression ratio at combustion duration of 60° for both propane-fuelled and the iso-octane-fuelled engine

Figure 38 shows the variation in bsfc with compression ratio separately for combustion duration of 100° for both propane-fuelled and the iso-octane-fuelled engine.

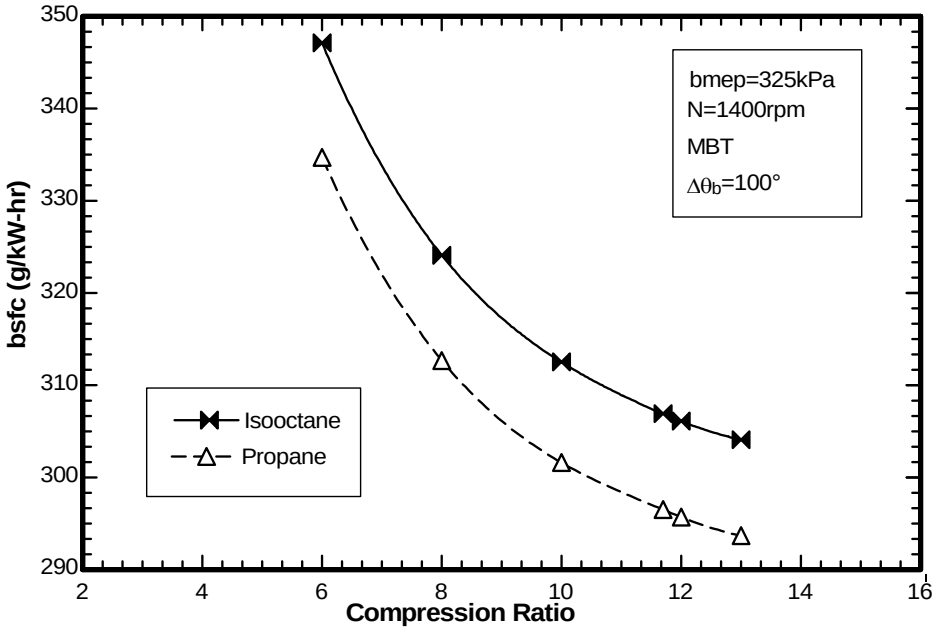

Fig. 38 Variation in brake specific fuel consumption (bsfc) with compression ratio at combustion duration of 100° for both propane-fuelled and iso-octane-fuelled engine

The effects of variations in compression ratio on brake thermal efficiency at three different combustion durations of 40°, 60°, and 100° for both propane-fuelled and the iso-octane-fuelled engine are shown in Figure 39. There is a consistent increase in the efficiency values with corresponding increase in compression ratio. This is inline with the expected general behavior as compression ratio has a direct bearing on the efficiency. The corresponding values of efficiency are approximately the same for both propane-fuelled and the iso-octane-fuelled engine.

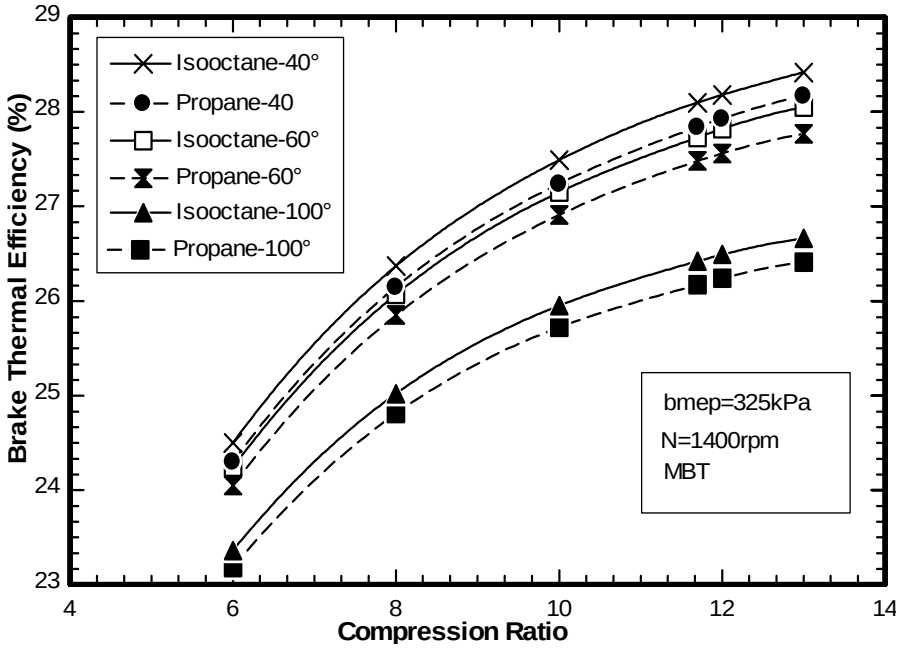

Fig. 39 Variation in brake thermal efficiency with compression ratio at combustion durations of 40°, 60°, and 100° for both propane-fuelled and iso-octane-fuelled engine

Figure 40 shows the individual variation in efficiency separately for the combustion duration of 60°. The difference between the thermal efficiency values for propane-fuelled and the iso-octane-fuelled engine is not significant. For the same brake specific fuel consumption of the two fuels, the thermal efficiency effectively becomes inverse function of calorific value of the fuel under consideration. Since, propane has a higher calorific value on a mass basis, therefore, it would result in lower efficiency.

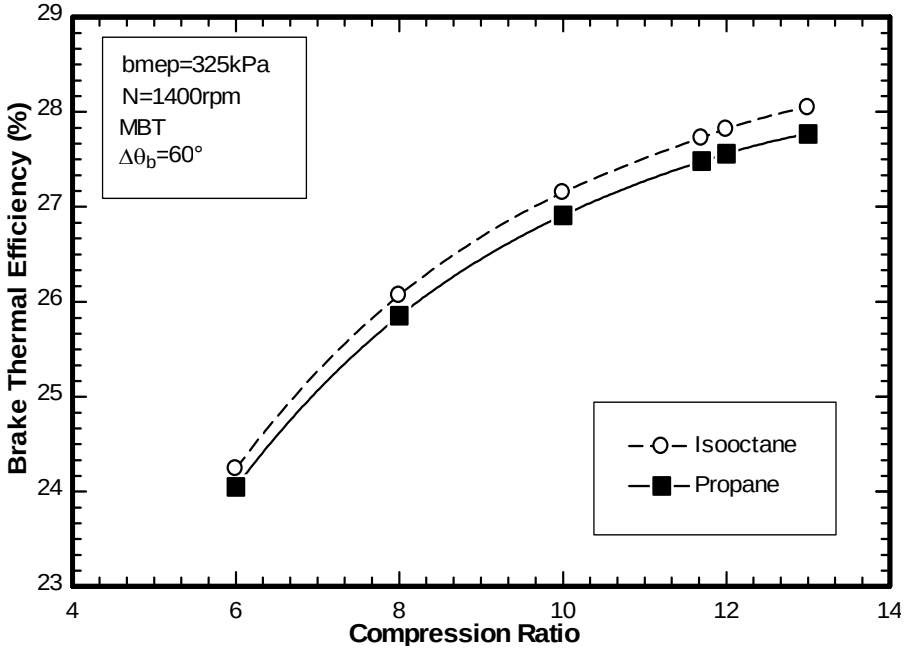

Fig. 40 Variation in brake thermal efficiency with compression ratio at 60° combustion duration for both propane-fuelled and the iso-octane-fuelled engine

The effects of variations in compression ratio on T_{exh} at three different combustion durations of 20°, 60°, and 100° for both propane-fuelled and the iso-octane-fuelled engine are shown in Figure 41. As the fuel conversion efficiency increases, the percentage of heat rejected through exhaust drops. This explains the drop in exhaust temperature with increase in compression ratio. The difference in the exhaust temperature temperatures for propane-fuelled and iso-octane-fuelled engine is due to the different exhaust mixture composition.

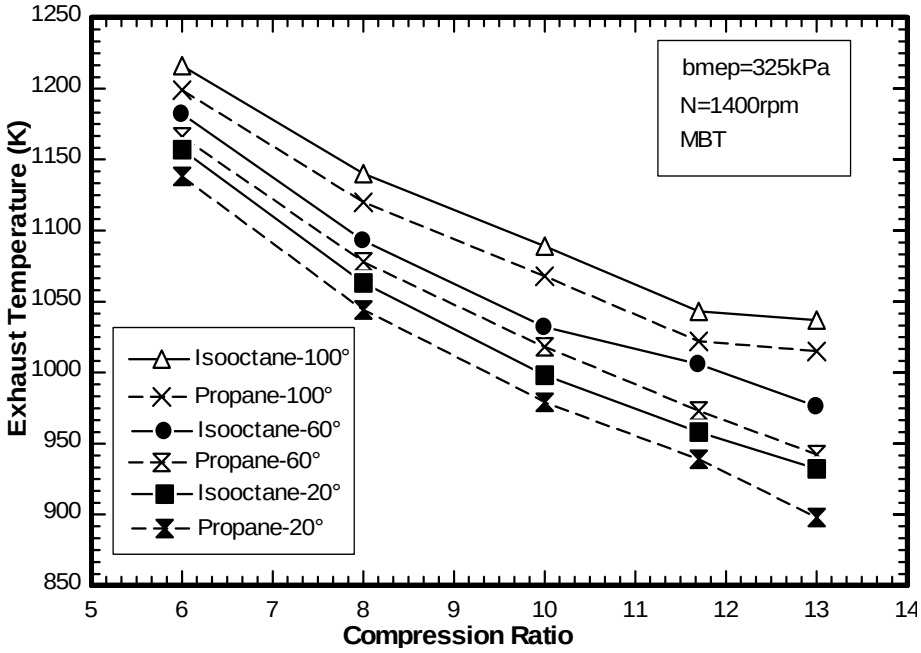

Fig. 41 Variation in mean exhaust temperature (T_{exh}) with compression ratio at combustion durations of 40°, 60°, and 100° for both propane-fuelled and the iso-octane-fuelled engine

Figure 42 shows the individual variation in T_{exh} with compression ratio separately for the combustion duration of 60° for both propane-fuelled and the iso-octane-fuelled engine. The difference in the exhaust temperatures for propane-fuelled and the iso-octane fuelled engine is due to the different exhaust mixture compositions.

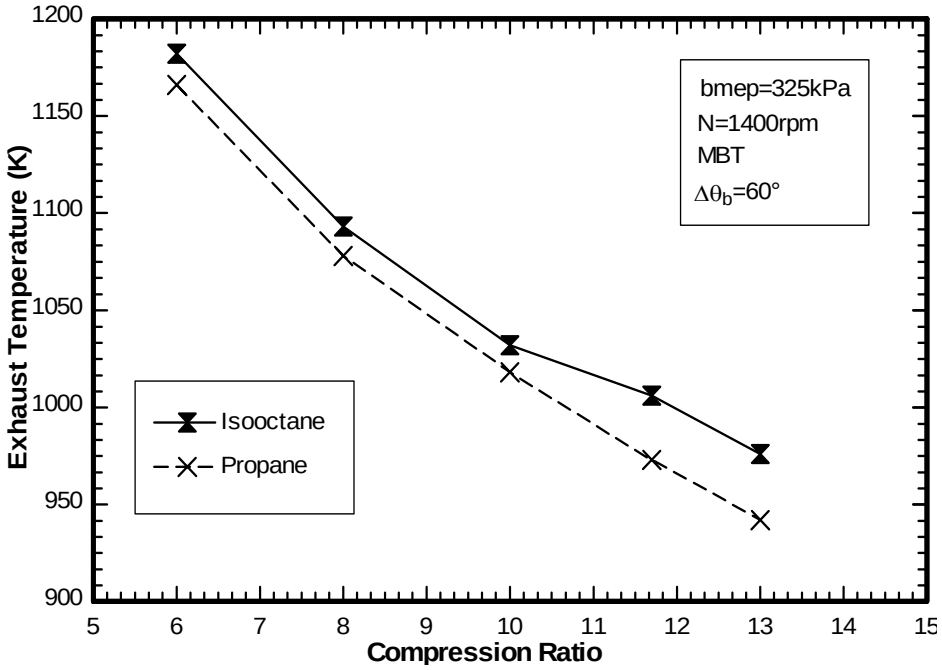

Fig. 42 Variation in mean exhaust temperature (T_{exh}) with compression ratio at combustion duration of 60° for both propane-fuelled and the iso-octane-fuelled engine

Figure 43 shows the percentage relative difference between the simulated and the experimentally determined values for bsNO and T_{exh} for the base case with variation in compression ratio.

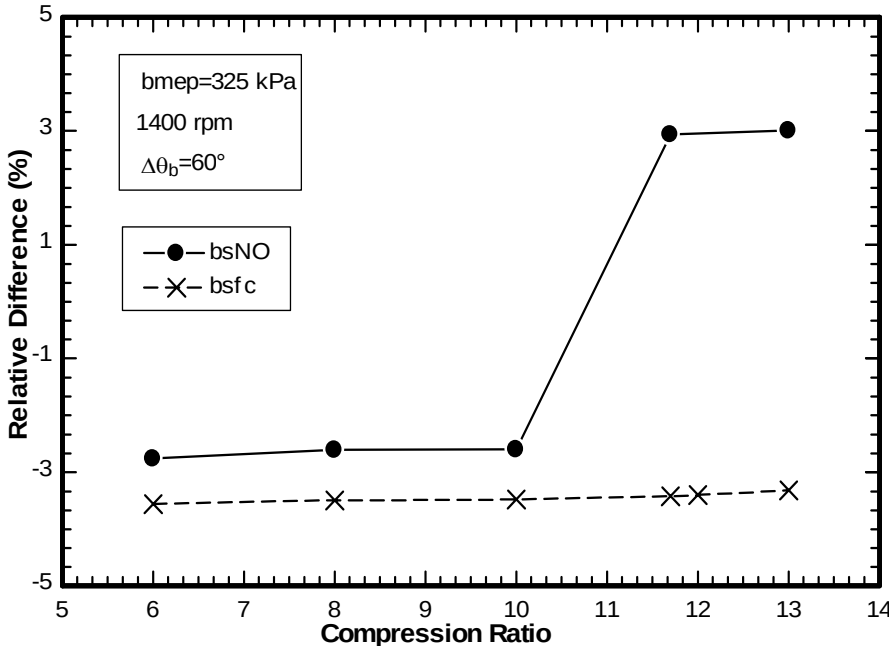

Fig. 43 Percentage relative difference between simulated and the experimental values of bsNO and bsfc with variation in compression ratio for the base case conditions

6.4.5 Load and Speed Variation

The effects of variations in engine speed on brake thermal efficiency at three different load conditions of 163 kPa, 325 kPa, and 655 kPa for both propane-fuelled and the iso-octane-fuelled engine are shown in Figure 44. The combustion duration is maintained constant at 60°. It is noted that the brake thermal efficiency values increase with corresponding increase in load for both propane-fuelled and the iso-octane fuelled engine. However, the relative difference between the corresponding values for the two fuels is negligible.

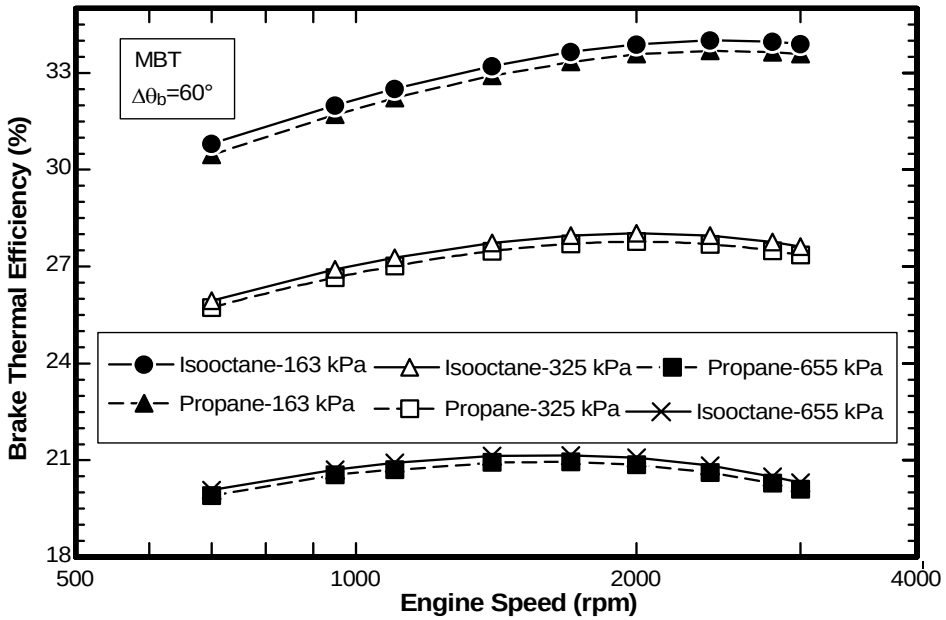

Fig. 44 Effect of variation in engine speed on brake thermal efficiency at three different load conditions for both propane-fuelled and iso-octane-fuelled engine

The effects of variations in engine speed on T_{exh} at three different load conditions of 163 kPa, 325 kPa, and 655 kPa for both propane-fuelled and iso-octane-fuelled engine are shown in Figure 45.

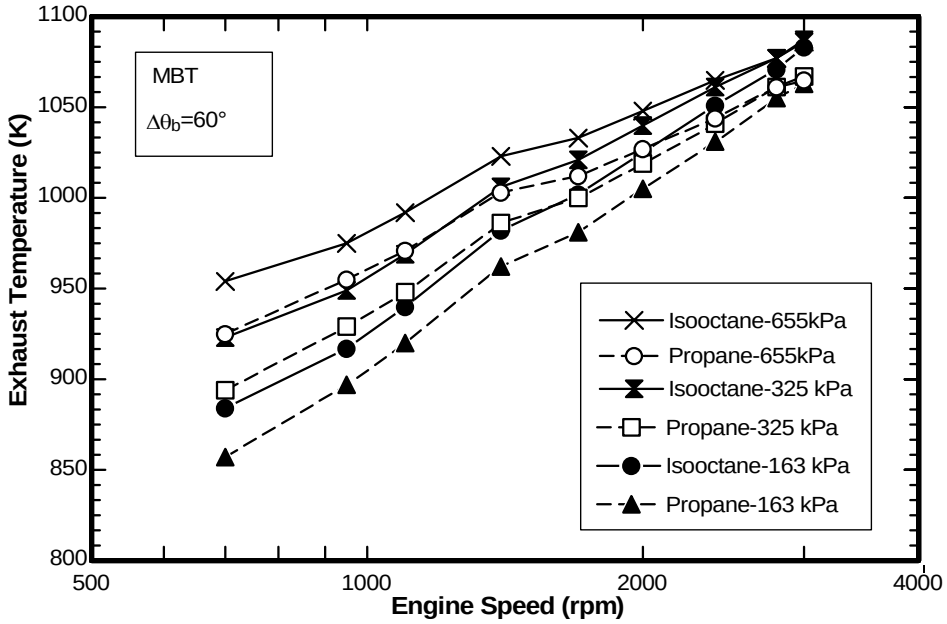

Fig. 45 Effect of variation in engine speed on mean exhaust temperature (T_{exh}) at three different load conditions for both propane-fuelled and the iso-octane-fuelled engine

For a clear understanding of the plots from Figure 45, individual plot for load condition of 325 kPa is presented separately for both propane fuelled and the iso-octane fuelled engine in Figure 46. The relative difference between the T_{exh} values for propane-fuelled and the iso-octane-fuelled engine becomes less significant at higher engine speeds, as shown in the figure.

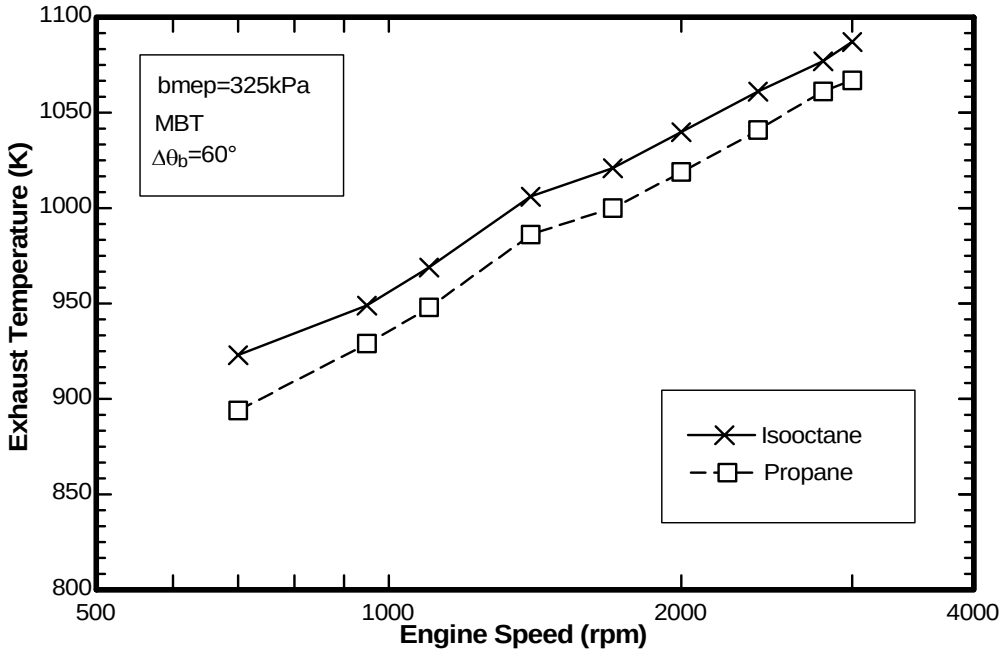

Fig. 46 Effect of variation in engine speed on mean exhaust temperature (T_{exh}) at load condition of 325 kPa for both propane-fuelled and the iso-octane-fuelled engine

7. SUMMARY, CONCLUSIONS, AND RECOMMENDATIONS

A thermodynamic cycle simulation of a four stroke spark-ignition engine was used to determine the difference in the engine performance parameters and emission characteristics between a propane-fuelled engine and an iso-octane-fuelled engine for the same operating conditions and engine specifications. Variation in brake specific fuel consumption, brake specific nitric oxide emissions, and mean exhaust temperatures with equivalence ratio, percentage exhaust gas recycle, spark timing, compression ratio, and engine speed and load were determined for both a propane-fuelled and an iso-octane-fuelled engine. Also, improvements were made in the friction mean effective pressure expressions. Results from the simulation were compared with the available experimental data and a good correlation was obtained between the simulated and the experimentally determined values.

The results of the parametric study can be summarized as below:

1. The bsfc values for the propane-fuelled engine were consistently lower (3 to 5 %) than the corresponding values for the iso-octane-fuelled engine for all the operating conditions and the parameters considered for the analysis. This observation is attributed to the fact that the calorific value of propane is higher than that of the iso-octane, resulting in a higher power output for the same mass of the two fuels. Low bsfc values are always desirable; however, it should not be concluded from the above observation that the fuel conversion efficiency of propane would be higher than that of iso-octane, as the efficiency is a function of calorific value of the fuel.

2. The bsNO values obtained for both propane-fuelled and the iso-octane-fuelled engine were approximately the same for all operating conditions and the parameters considered for the investigation. This observation can be attributed to their near similar peak combustion temperatures for all operating conditions. This observation re-establishes the fact that the formation of NO_x is primarily a function of peak combustion temperature.

3. The mean exhaust temperature values for the propane fuelled engine were consistently lower (2 to 3 %) than the corresponding values for the iso-octane fuelled engine over the entire range of operating conditions and the parameters selected for the investigation. This observation is a consequence of the different exhaust mixture compositions resulting from the two fuels.

4. Another observation from the parametric investigation is that the combustion duration does not have a bearing on bsfc, bsNO, and T_{exh} values in terms of the relative difference for propane fuelled and iso-octane fuelled engine. It was observed that the relative difference in the engine performance parameters between the propane-fuelled and iso-octane-fuelled engine were similar for combustion durations of 20°, 60°, and 100°.

5. The improved friction model provided lower values of mechanical friction mean effective pressure and the gas loading effect. However, friction mean effective pressure (fmep) was an input to the simulation program and the fmep values obtained from the improved model were used for both propane-fuelled as well as the iso-octane-fuelled engine to maintain the same operating conditions. Therefore, the improved model did not have any bearing on the predicted results for both propane-fuelled and the iso-octane-fuelled engine.

Based on the summary of the results, it is observed that the values of the engine performance parameters (bsfc, and T_{exh}) and NO_x emissions characteristics for the propane-fuelled and the iso-octane-fuelled engine are approximately the same throughout the operating range. A relative difference of 3 to 5 % in the bsfc values, 2 to 3 % in the T_{exh} values and 1 to 3 % in the bsNO values was obtained between the propane-fuelled and iso-octane-fuelled engine. From a practical stand point, this difference is extremely small and can be regarded as insignificant. But the encouraging observation lies in the fact that a compression ratio of 11.7 was used for all the computations in the present work, for both the propane-fuelled and the iso-octane-

fuelled engine. In practice, a compression ratio of 11.7 would not be recommended for an iso-octane-fuelled engine because of the knocking phenomenon. On the other hand a propane-fuelled engine would operate well at this compression ratio because of its higher octane number rating. This implies that the engine performance and NO_x emissions from a propane-fuelled engine would be similar to that from an iso-octane-fuelled engine if higher compression ratios are used.

The main conclusion from this study lies in the fact that because of propane's higher octane number rating, it can be used in engines with higher compression ratios and provide engine performance similar to that from an iso-octane fuelled engine.

The recommendations for the future work are stated below:

1. Previous experimental studies have indicated that the fuel's chemical structure has a more profound effect on the HC and CO emissions than on NO_x formation. Therefore, the effect of fuel structure and engine parameters on the formation of HC and CO should be determined.

2. Other alternative fuels such as methane, methanol, and ethanol should be considered for a similar investigation.

REFERENCES

1 **Thring, R. H.** Alternative fuels for spark-ignition engines. SAE paper 831685, 1983.

2 **Nichols, R. J.** The challenges of change in the auto industry: Why alternative fuels?. In Proceedings of the 15th Annual Fall Technical Conference of the *ASME Internal Combustion Engine Division*, Morgantown, West Virginia, 26-29 September, 1993, pp. 3-10.

3 U.S. Department of Energy, Alternative Fuels Data Center, Available: http://www.eere.energy.gov/afdc/, Accessed: 09/19/2005.

4 **Larsen, R.** and **Buitrago, C.** 1996 Propane vehicle challenge. In Proceedings of the 1997 International Congress and Exposition, Detroit, Michigan, 24-27 February, 1997, pp. 31-43.

5 **Patton, K. J., Nitschke, R. G.,** and **Heywood, J. B.** Development and evaluation of a performance and efficiency model for spark-ignition engines. SAE paper 890836, 1989.

6 **Sandoval, D.** and **Heywood, J. B.** An improved friction model for spark-ignition engines. SAE paper 2003-01-0725, 2003.

7 **Flynn, P. F., Hunter, G. L., Farrel, L, Durrett, Akinyemi, O., Loye, A. O., Westbrook, C. K.,** and **Pitz, W. J.** The inevitability of engine-out NO_x emissions from spark-ignited and diesel engines. In Proceedings of the 28th International Symposium on Combustion, Edinburgh, United Kingdom, 30 July - 4 August, 2000, pp. 1211-1217.

8 **Kaiser, E. W., Siegl, W. O., Henlg, Y. I., Anderson, R. W.,** and **Trinker, F. H.** Effect of fuel structure on emissions from a spark-ignited engine. *Environmental Science and Technology*, 1991, **25**, 2005-2012.

9 **Cotton, K. J.** A study of the potential of propane fuel to reduce utility engine exhaust emissions. SAE paper 921696, 1992.

10 **Baker, P.**, and **Watson, H.** MPI air/fuel mixing for gaseous and liquid LPG. SAE paper 2005-01-0246, 2005.

11 **Lu, J., Gupta, A. K.,** and **Keating, E. L.** Effect of engine operating parameters on combustion and emission characterstics. In Proceedings of the 1992 ASME International Computers in Engineering Conference and Exposition, San Francisco, California, 2-6 August, 1992, pp. 669-675.

12 **Smith, J., Celik, I.,** and **Lyons, D. W.** Prediction of emission trends from a SI engine with alternative fuels. In Proceedings of the 1996 18th Annual Fall Technical Conference of the *ASME Internal Combustion Engine Division*, Fairborn, Ohio, 20-23 October, 1996, pp. 89-97.

13 **Yamin, J. A.,** and **Badran, O. O.** Analytical study to minimize the heat losses from a propane-powered four-stroke spark ignition engine. *Renewable Energy*, 2002, **27**, 463-478.

14 **Heywood, J. B.** *Internal Combustion Engines Fundamentals*, 2000 (McGraw Hill, New York).

15 **Heywood, J. B., Higgins, J. M., Tabaczynski, R. J.,** and **Watts, P. A.** Development and use of a cycle simulation to predict SI engine efficiency and NO_x emissions. SAE paper 790291, 1979.

16 **William, J. A.** *Engineering Tribology*, 1994 (Oxford University Press, New York).

APPENDIX 1

PROPERTIES OF VARIOUS FUELS [3]

Property	*Gasoline*	*Diesel*	*Methanol*	*Ethanol*	*Propane*	*Methane*
Chemical Formula	C_4-C_{12}	C_3-C_{25}	CH_3OH	C_2H_5OH	C_3H_8	CH_4
Density (lb/gal) @ 60° F	6.0-6.5	6.7-7.4	6.63	6.61	4.22	1.07
Octane Number (R+M)/2	86-94	NA	100	100	104	120+
Auto-ignition Temperature (°F)	495	≈600	867	793	850-890	1004
Latent Heat of Vaporization (Btu/gal)	≈900	≈700	3,340	2,378	775	-
Lower Heating Value (Btu/gal)	115,000	128,400	56,800	76,000	84,500	19,800
Lower Heating Value (Btu/lb)	18,000-19,000	18,000-19,000	8,570	11,500	19,800	21,300

APPENDIX 2

VISCOSITY DATA FOR VARIOUS OIL GRADES [4]

Oil Grade	*k (cSt)*	θ_1 (°C)	θ_2 (°C)	μ_∞/μ	c_1	c_2
0W40	0.01341	1986.4	189.7	0.67	2.5	0.026
5W20	0.04576	1224	134.1	0.94	2.5	0.029
5W40	0.15	1018.74	125.91	0.8	2.3	0.0225
10W30	0.1403	869.72	104.4	0.76	2.3	0.0225
10W50A	0.0352	1658.88	163.54	0.49	2.43	0.0218
10W50B	0.0507	1362.4	129.8	0.52	2.28	0.0269
15W40A	0.1223	933.46	103.89	0.9	2.3	0.0225
15W40B	0.03435	1424.3	137.2	0.79	2.5	0.026
20W50	0.0639	1255.46	117.7	0.84	2.3	0.0225
SAE10	0.0258	1345.42	144.58	1	2.3	0.0225
SAE30	0.0246	1432.29	132.94	1	2.3	0.0225
SAE50	0.0384	1349.94	115.16	1	2.3	0.0225

APPENDIX 3

FRICTION PREDICTIONS FROM THE IMPROVED MODEL

As documented earlier, several modifications were made to the friction terms representing the gas pressure loading. Figures 47 to 49 show the effects of these modifications on gas load fmep with variation in inlet pressure, engine speed, and compression ratio respectively. The values predicted by the improved model are lower than the corresponding values from the previous model.

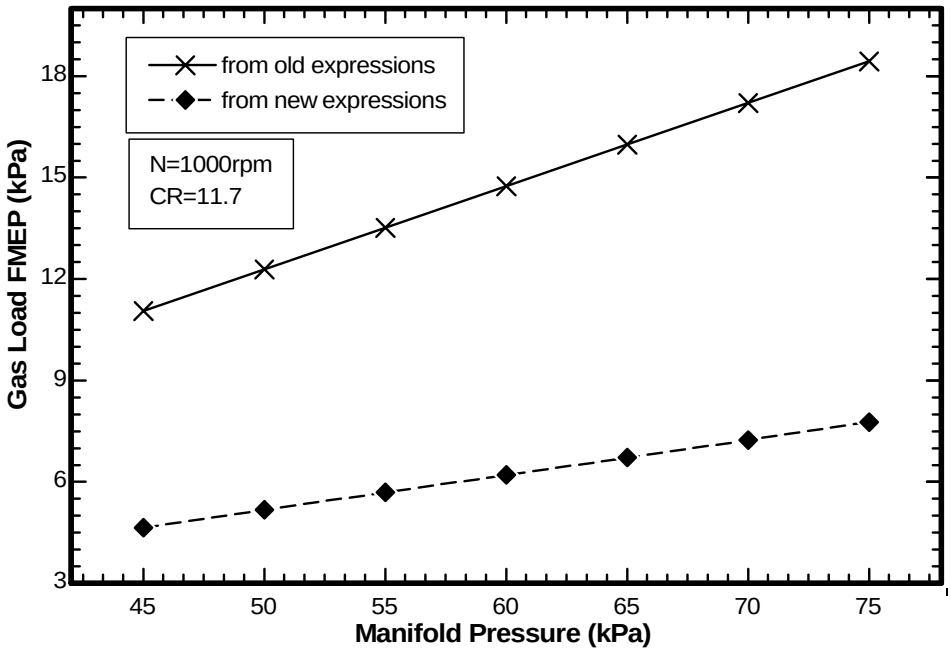

Fig. 47 Variation in gas load friction mean effective pressure with inlet pressure at constant speed and fixed engine geometry

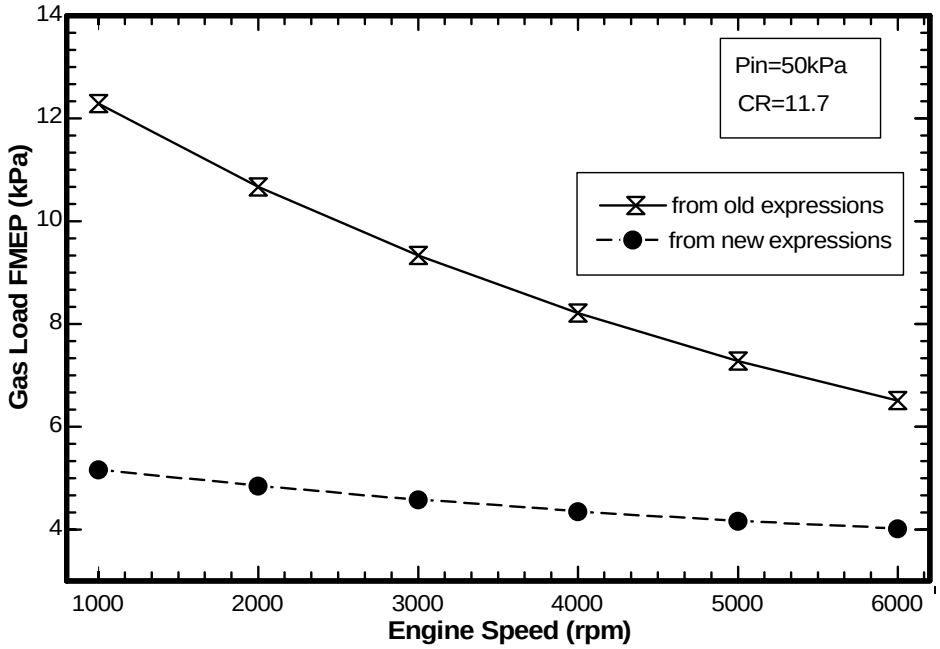

Fig. 48 Variation in gas load friction mean effective pressure with engine speed for a fixed engine geometry and inlet pressure

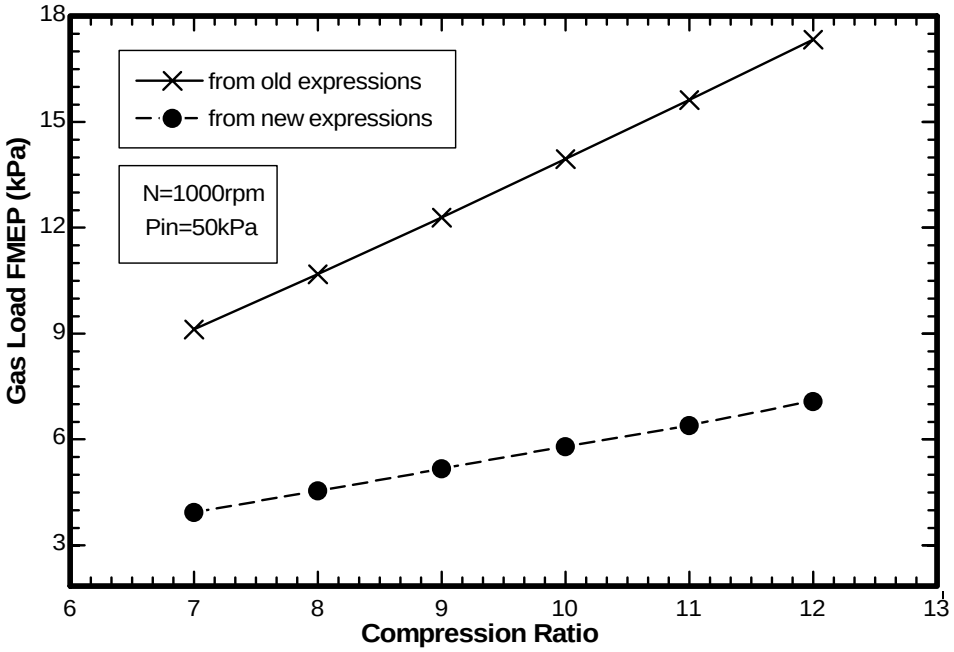

Fig. 49 Variation in gas load friction mean effective pressure with compression ratio at constant speed and fixed inlet pressure

Figure 50 shows the effect of variation in engine speed on pumping mean effective pressure (pmep) for a fixed engine geometry and constant inlet pressure. The figure includes plots obtained from the improved model as well as the original model. Predictions made by the improved model are lower in the engine speed range of 3000 to 6000 rpm.

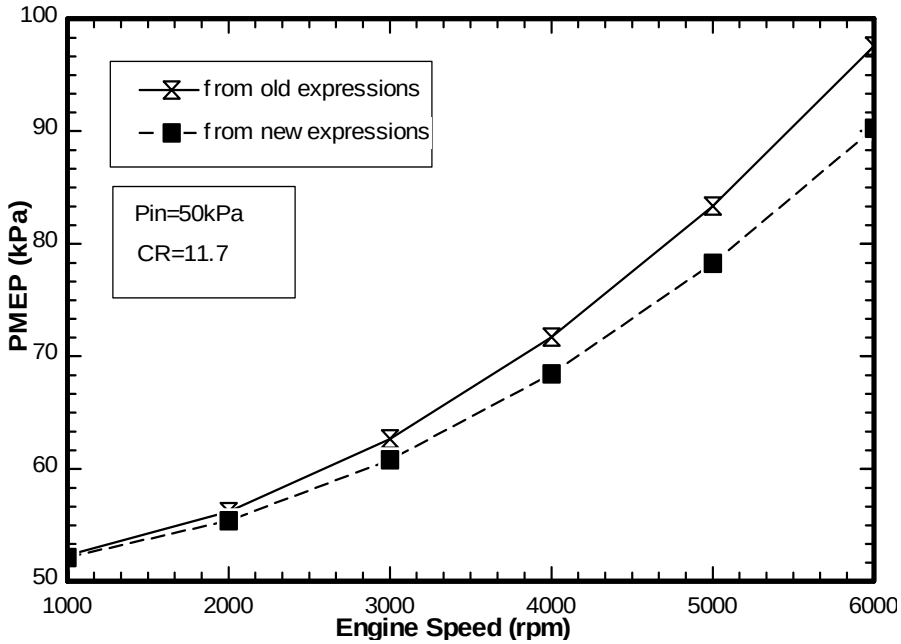

Fig. 50 Variation in pumping mean effective pressure with engine speed at fixed engine geometry and fixed inlet pressure

Figure 51 shows the effects of modifications on the total mechanical mean effective pressure (mfmep). The figure shows the variation in mfmep with engine speed for a fixed engine geometry and constant inlet pressure. Plots from both the improved and the original model are presented in the figure. The improved model predicts lower mfmep values in the low engine speed range (below 2500 rpm).

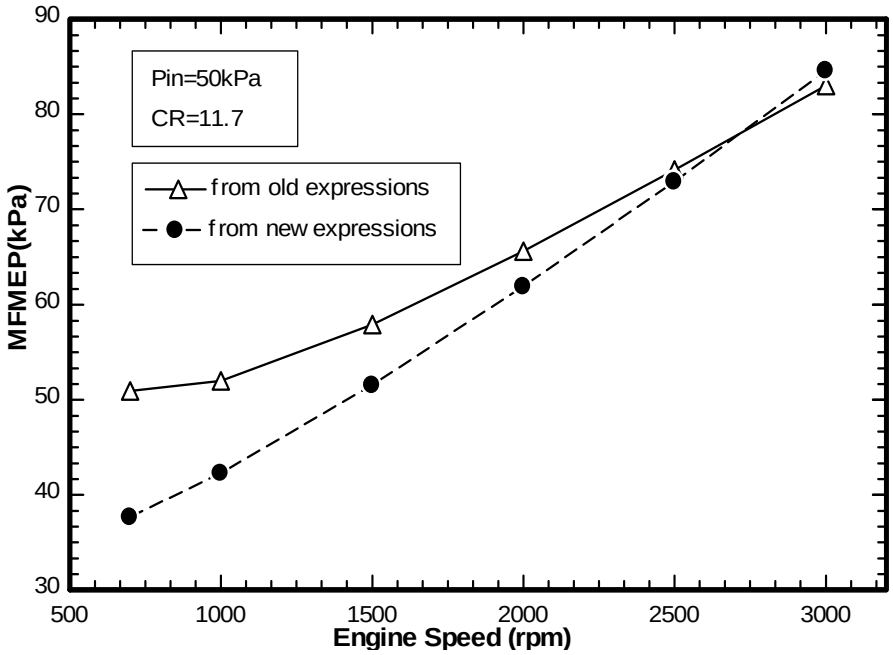

Fig. 51 Variation in mechanical friction mean effective pressure (mfmep) with engine speed for a fixed engine geometry and fixed inlet pressure

VITA

Name: Dushyant Pathak

Address: Texas A&M University, Department of Mechanical Engineering, 3123 TAMU, College Station, TX 77843-3123.

Education: Master of Science, Mechanical Engineering, December 2005
Texas A&M University, College Station, TX.

Bachelor of Technology, Mechanical Engineering, June 2002
R E C Kurukshetra, Kurukshetra University, Haryana, India.